Theoretical model Predictions of medically important ^{88}Y, ^{89}Zr, ^{90}Y and ^{99}Mo radionuclides produced in α induced reaction at ≈10-60MeV

A Thesis Submitted to School of Graduate Studies College of Natural and Computational Science in Partial Fulfillment of the Requirements for the Degree of Master of Science in Physics.

By:

Negash Gimbo

Hawassa, Ethiopia

May, 2024

Declaration

I hereby declare that this MSc Thesis is my original work and has not been presented for a degree in any other university, and that all sources of material used for the thesis have been duly acknowledged.

Name: Signature:

Negash Gimbo ______________________

Email: nege811@gmail.com

This MSc thesis has been submitted for examination with my approval as university advisor.

Name: signature:

Amanuel Fessahatsion (PhD) ______________________

Place and date of submission:

Hawassa, Ethiopia

May, 2024

Hawassa University

Schools of Graduate Studies

Examiner's Approval Sheet

We, the undersigned, members of the broad of examiners of the final open defense by Negash Gimbo Mekisa have read and evaluated his thesis in entitled "**Theoretical model Predictions of medically important ^{88}Y, ^{89}Zr, ^{90}Y and ^{99}Mo radionuclides produced in α + ^{89}Y, ^{96}Zr induced reaction at ≈10-60 MeV"** and examined the candidate. This is therefore to certify that the thesis has been accepted in partial fulfillment of the requirement for the degree of Masters in Physics.

____________________	_______________	______________
Name of Major Advisor	Signature	Date
____________________	_______________	______________
Name of Internal Examiner- I	Signature	Date
____________________	_______________	______________
Name of Internal Examiner -II	Signature	Date
____________________	_______________	______________
Name of External Examiner	Signature	Date
____________________	_______________	______________
SGS Approval	Signature	date

Finally approval and acceptance of the thesis is contingent up on the submission of the finally copy of the thesis to the school of Graduate studies (SGS) through the Department/School graduate committee (DGC/SGS) of the candidate's department.

Stamp of SGS Date: ________________

Hawassa University

College of Natural and Computational Sciences

Department of Physics

Advisor Approval sheet.

The undersigned hereby certify that they have read and recommend to the College of Natural and computational Science School of Graduate Studies for acceptance MSc Thesis entitled "**Theoretical model Predictions of medically important ^{88}Y, ^{89}Zr, ^{90}Y and ^{99}Mo radionuclides produced in $\alpha + ^{89}$Y, ^{96}Zr induced reaction at ≈10-60 MeV**" by author Negash Gimbo in partial fulfillment of the requirements for the degree of Masters in Physics.

Approved by:

Name of Advisor	Signature	Date
______________________	______________	______________
Department Head	Signature	Date
______________________	______________	______________

Acknowledgement

First of all, I would like thank the Almighty God. Next I would like to thank my advisor Dr. Amanuel fessahatsion for his skilful guidance, professional support and encouraging ideas. His helpful comments and suggestions based on extensive knowledge of research experience prepared me for the research. I am grateful to all my family members especially my mother for her love and support. I also thank my former class mate Tiguaded Yeneabat and her friend yegnanesh fenta for their help. I have obtained material from many scientific journals and books and I am grateful to the authors of these publications and books. Finally, I would like to thank the department head of physics Ato Wubshet Baharu, for all his support during my studies.

Abstract

In this work, theoretical predicted production cross section were made using COMPLETE, EMPIRE-3.2 and TALYS-1.95(G) reaction model codes for the production of medically important ^{88}Y, ^{89}Zr, ^{90}Y and ^{99}Mo radionuclides in the interaction of α-projectile with ^{89}Y and ^{96}Zr-targets at ≈10-60 MeV. The theoretical predicted production cross sections were compared with the experimental data available in the EXFORE database. The TALYS-1.95(G) code predicted production cross sections of medically important ^{88}Y, ^{90}Y, and ^{89}Zr radionuclide, in general, are found to be in good agreement with experimental measured production cross sections over the entire energy range except for ^{99}Mo radionuclide. Pearson's statistical coefficients confirmed a strong positive correlation between TALYS-1.95(G) codes predicted and experimentally measured production cross section except for ^{99}Mo. Furthermore, it was found that the TALYS-1.95(G) predicted and experimentally measured production cross-sections in general attained maximum values below ≈45MeV α-energy for medically important ^{88}Y, ^{90}Y, and ^{89}Zr radionuclides via complex (α,x) channel. Thus the obtained result can be used as reference cross-section data for optimized production of medically important ^{88}Y, ^{90}Y, ^{89}Zr and ^{99}Mo radionuclides using single α + ^{89}Y, ^{96}Zr system.

Table of contents **pages**

List of Table

List of Figures

List of Acronyms and Abbreviation

FGM	Fermi gas model
GSM	Generalised super fluid model
EGSM	Enhanced generalized super fluid model
OM	Optical model
EM	Exciton model
CN	Compound nucleus
PE	Pre-equilibrium
EF's	Excitation function
E_{proj}	Projectile energy
RIPL	Reference input parameter library
MFM	Mean Free Path Multiplier
PET	Positron emitted tomography
SPECT	Single positron emission computed tomography
TENDL	Talys based evaluated nuclear data library
EMPIRE	Exciton model program for induced reaction and emission
MeV	Mega electrovolt

Chapter One

Introduction

The exploration of the characteristics of atomic nuclei and the fundamental principles governing their interactions serves as the foundation for all nuclear technologies [1]. Significant findings have been obtained in the examination of nuclear reactions induced by alpha particles particularly in relation to reaction cross-sections [2]. A nuclear reaction involves the generation of new nuclei and elementary particles as particles and nuclei interact [3]. Hence, it is crucial to accurately measure and calculates the cross-sections of nuclear reactions and comprehends the mechanisms behind these reactions. The discernment of reaction mechanisms is derived from the analysis of differences in reaction cross-sections data revealing the properties and structures of nuclei that have valuable applications, such as fusion, fission, accelerator-driven systems, dosimetry, and nuclear medicine [4, 5]. These data are very important in radionuclide production, particularly for medically useful radionuclides [5].

In the realm of medical radiobiology, nuclear reaction cross-section data are most importance for both diagnostic imaging and targeted therapy. These data facilitate the optimization of established and new nuclear reaction routes, a critical aspect in the production of radionuclides [6]. Artificially produced radionuclides have extensive applications in agriculture, medicine, industry, and nuclear research [7]. Notably, over 100 radioactive substances are reported to be employed in nuclear medicine for therapeutic, diagnostic, and research purposes [8, 9]. Particularly, production of medical radionuclides using α-projectile are important, these radionuclides can be produced only via α-induced reactions with high-spin isomeric states, which are of interest in localized internal radiotherapy. Furthermore, α-induced reactions produce radionuclides two charge units higher than the target nuclei make the chemical separation more specific and the product can be obtained with very high radiochemical and chemical purity, which is significant in the production of metallic therapeutic radionuclides [2]. In this regard theoretical model predictions play a crucial role in developing optimized reference cross-section data, especially in the production of medically valuable radionuclides [10].

Accordingly, theoretical model-based comparative studies with experiments using light-ion projectiles (deuterons and α) are crucial [11-14] because of the limited experimental cross-section data to produce medical radionuclides, particularly in α-induced reactions where further investigations still demanding [11, 15].

Murata et al., [16] conducted a study on alpha-induced reactions involving ^{89}Y, specifically examining the excitation functions of ^{89}Zr and ^{90}Nb, which are applicable for immune-PET studies. The investigation employed the stacked-foil method, activation technique, and off-line gamma-ray spectrometry. Excitation functions for isotopes such as $^{92m, 91m, 89m}$, ^{89g}Nb, ^{88}Zr, $^{90m, 88g, 87m, 87g}$Y were derived and compared with both previous experimental data and the TENDL-2017 database. The study revealed good agreements with certain aspects of earlier research.

Additionally, Aikawa et al., [17] studied into the production of ^{117m}Sn through charged-particle induced reactions, a topic of interest for medical applications. The production cross-sections of alpha-induced reactions on ^{nat}In for ^{117m}Sn were investigated up to 50 MeV, employing the stacked foil technique and activation method. The integral yield of ^{117m}Sn was estimated based on the measured cross-sections, and the results were compared with both previously explored experimental data and theoretical calculations. The study also presented measured cross-sections for isotopes such as ^{113}Sn and $^{116m, 117, 118m}$ Sb.

Tárkányi et al., [18] investigated the production of medical important ^{44}Sc(^{44}Ti), ^{52m}Mn(^{52}Fe), ^{52g}Mn, ^{55}Co, ^{61}Cu, ^{62}Cu(^{62}Zn), ^{66}Ga, ^{68}Ga(^{68}Ge), ^{72}As(^{72}Se), ^{73}Se, ^{76}Br, ^{82}Rb(^{82}Sr), ^{82m}Rb, ^{86}Y, ^{89}Zr, ^{90}Nb, ^{94m}Tc, ^{110m}In(^{110}Sn), ^{118}Sb(^{118}Te), ^{120}I, ^{122}I(^{122}Xe), ^{128}Cs(^{128}Ba), and ^{140}Pr(^{140}Nd) radionuclides produced in various projectiles + targets reactions up to 50MeV energy. The investigation particularly focused on diagnostic positron emitters radionuclides. Reference cross-section data were derived from Padé fits applied to select and corrected experimental data, and integral thick target yields were subsequently calculated. To account for uncertainties in the fitted results, a Padé least-squares method was employed, with an additional 4% systematic uncertainty assessed. The experimental data were further compared with theoretical predictions available from the TENDL-2015 and TENDL-2017 libraries, sometimes exhibiting significant disagreements in the magnitude and shape of the resulting excitation functions. As well as a lack of published data for specific reactions, significant disagreements were also found to exist between various equivalent experimental data. All of the recommended cross-section data were used to derive integral or production thick target yields for direct practical application.

All of the numerical reference cross-section data with their corresponding uncertainties were deduced. These evaluated experimental data are important for existing and potential applications in nuclear medicine, and may also have useful roles in other fields of non-energy related nuclear studies.

Aslam et al., [19] investigated the optimized production of medically useful ^{68}Ga radionuclides produced in the interaction of α –projectile with enriched ^{65}Cu-target at energies below 40 MeV. For the production of ^{68}Ga radionuclide via ^{65}Cu (α, n) ^{68}Ga reaction, a good agreement was achieved between the measured data and the TALYS 1.95 calculated cross sections. The generated recommended production cross section provided thick target yield for the ^{65}Cu (α, n) ^{68}Ga reaction. The obtained result further suggested that the ^{65}Cu (α, n) ^{68}Ga reaction is a potential route for the production of ^{68}Ga at low energy cyclotrons due to no radio-impurities in the region of 7 MeV - 14 MeV.

Recently, Amanuel [20] studied into the nuclear model predictions of medically important radionuclides, including ^{22}Na, ^{51}Cr, ^{60}Co, ^{61}Cu, ^{64}Cu, ^{65}Zn, ^{67}Ga, ^{68}Ga, ^{88}Y, and ^{99}Mo. These radionuclides were produced through α-induced reactions utilizing various projectile-target systems within the energy range of 10-65MeV. The theoretical analyses and comparisons were conducted using the ALICE/ASH and EMPIRE 3.2 reaction model codes. The finding revealed that general trend across all (α, x) and (α, n) reaction channels, where the production cross-sections initially increased with rising α-projectile energy, reached a maximum value, and then decreased as a function of α-projectile energy. The study indicated that the predicted and measured cross-sections for the production of medically important radionuclides, such as ^{51}Cr, ^{64}Cu, ^{65}Zn, ^{68}Ga, and ^{99}Mo, were generally similar in magnitude over their respective energy ranges. Moreover, the obtained results suggested that the prediction of EMPIRE 3.2 code can be used as reference cross section data in pushing a well-controlled and optimized production of medical radionuclides below 40 MeV.

In the past various investigations on the productions of medically important radionuclides have been carried out using α-projectile; however, reasonable comparative production cross section studies between theory and experiment of medically important radionuclides produced in α-induced reactions have not been investigated efficiently and still need further investigations [1, 11, 21, 22, 23].

Accordingly, the present work attempts to contribute to addressing the gaps identified above excitation functions of medically used radionuclides such as ^{88}Y, ^{89}Zr, ^{90}Y and ^{99}Mo radionuclides produced in α induced reaction at ≈10-60MeV. For theoretical predictions reaction model codes COMPLETE, EMPIRE-3.2 and TALYS-1.95(G) were used.

1.1. Objectives of study

1.1.1. General objective

- To predict the production of medically important **^{88}Y, ^{89}Zr, ^{90}Y and ^{99}Mo** radionuclides produced in α + ^{89}Y, ^{96}Zr induced reactions at ≈10-60 MeV

1.1.2. Specific objectives

- ✓ To optimize the theoretical model codes input parameters to produce the measured data
- ✓ To find the correlation between the predicted and measured production cross sections
- ✓ To find the projectile energy point that produced the optimized production cross-section

Chapter Two

Theoretical Background

2.1. Nuclear reaction

A nuclear reaction refers to a process in which one or more nuclides are produced as a result of the collision between atomic nuclei or between one atomic nucleus and a subatomic particle. This phenomenon involves the transformation of atomic nuclei through the influence of particles such as neutrons, protons, deuterons, or radiation such as α, β, and γ radiation. While nuclear reactions can occur spontaneously in the nuclei of natural or artificially radioactive substances, they can also be induced artificially by bombarding the atomic nucleus with particles or radiation [24].

In the definition of a nuclear reaction, it is specified that the process occurs when the bombarding particle and a nucleus come into close contact, typically within a distance of about 10^{-15} meters [25]. Consequently, the energy involved in the reaction must be sufficiently high to overcome the natural electromagnetic repulsion between the protons of the incident and target nuclei, and this energy barrier is commonly referred to as the Coulomb barrier [26]. If the energy falls below this barrier, the nuclei will repel each other. Notably, early experiments conducted by Rutherford utilized low-energy alpha particles from naturally radioactive material to collide with target atoms, measuring the size of the target nuclei. These experiments were conducted at bombarding energies below 100 MeV.

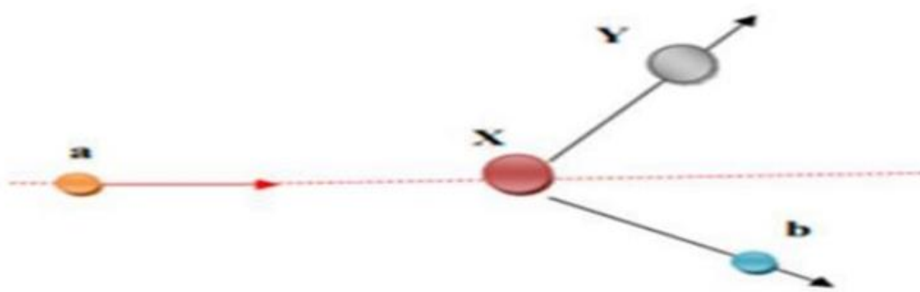

Fig 2.1 Schematic representation of a nuclear reaction [27]

$$a + X \rightarrow b + Y + Q \qquad (2.1)$$

In short way of the above reaction is; X (a; b) Y [27].

If more than one particle say b_1, b_2 and b_3 are emitted then the reaction is written as [25]

$$a + X \rightarrow Y + b_1 + b_2 + b_3 \qquad (2.2)$$

It denoted as X (a; $b_1b_2b_3$) Y

Where a is the bombarding particle (projectile), X =target nucleus, Y = Residual nucleus, b = outgoing particle, Q = the energy released in the reaction and is given by

$$Q = (M_a + M_x)C^2 - (M_y + M_b)\,C^2 \qquad (2.3)$$

In which M_a =mass of the projectile, M_x = mass of the target nucleus, M_y = mass of the residual nucleus, M_b =mass of the released particle (ejectile), C =the speed of light

In nuclear reactions, the projectile can take various forms such as a proton, neutron, deuteron, alpha particle, or any other heavy ions. The emitted particles from these reactions may include nucleons, a nucleus, or gamma radiations. The study of nuclear reactions holds significant importance as it provides detailed information about nuclear mass, charge distribution, nuclear force, and, more broadly, the nuclear structure and reaction mechanisms. The outcomes of these reactions may involve the emission of different particles, including nucleons and nuclei. During the collision between the projectile particle and a target nucleus, one of the following events typically occurs [27]. i) The beam particle scatters elastically, leaving the target nucleus in its ground state. ii) The target nucleus becomes internally excited and subsequently decays by emitting radiation or nucleons. To describe nuclear reactions more comprehensively, a set of equations can be employed. These equations offer a means to articulate the intricate details of the various events that unfold during nuclear reactions.

$$a + X \rightarrow X + a \qquad (2.4)$$

$$\rightarrow X^* + a$$

$$\rightarrow Y + b$$

$$\rightarrow Z + c \quad \text{e t c.}$$

As evident from the first two reactions, when the outgoing particle is of the same type as the incident particle, the process is referred to as scattering. In the first reaction, elastic scattering occurs, where the total kinetic energy of the system (projectile plus target nucleus) remains the same both before and after the collision. Conversely, in the second reaction, inelastic scattering takes place, causing the target nucleus X to be raised into an excited state. In this scenario, the total kinetic energy of the system decreases by the amount of excitation energy transferred to the target nucleus.

The excited product nucleus typically undergoes rapid decay to the ground state by emitting gamma rays. A landmark moment in the history of nuclear reactions occurred in 1919 when Lord Rutherford conducted the pioneering experimental observation of a nuclear reaction. This groundbreaking experiment involved directing an alpha particle onto the nucleus of a nitrogen target [27, 28].

In the context of producing radionuclides using accelerators, the outcome of the reaction is depend upon both the energy threshold and the cross section, with the latter being influenced by the energy of the incoming projectile. Accelerators typically employ light charged particles such as protons, deuterons, ^{3}He, or α particle as bombarding particles. The characterization of a nuclear reaction X (a, b) Y is commonly expressed in terms of the cross section, a parameter that fundamentally reflects the Probability of the reaction occurring and can be calculated [29].

$$a + {}^{A}_{Z}X \rightarrow {}^{A}_{Z}Y + b + Q \qquad (2.5)$$

Conservation laws play a crucial role as fundamental prerequisites for the occurrence of a reaction, and nuclear reactions are basically governed by these laws. Therefore, the analysis of any nuclear reaction consistently involves the application of conservation laws both before and after the reaction occurs. Key quantities that must be conserved include mass, energy, momentum, angular momentum, charge, the number of nucleons, spin parity, and isospin. With the exception of high-energy reactions leading to meson production, the conservation of the number of neutrons and protons is a constant feature in nuclear reactions [30, 31].

In a typical nuclear reaction, a projectile α is incident on a target nucleus A and after the collision a nucleus B and an outgoing particle b are observed. This is written as

$$A + a \rightarrow b + B \text{ or } A\ (a, b)\ B \qquad (2.6)$$

Particles denoted as a and b can take various forms such as photons, electrons, mesons, nucleons, or nuclei. When both a and b are nuclei, the collision is referred to as a heavy ion reaction. The foundational theory for describing nuclear reactions is quantum theory. In this theoretical framework, specific quantum numbers associated with the relative motion between the particles, the types of particles involved, and their intrinsic quantum numbers (such as individual angular momenta or nuclear spins) are considered. The term "reaction channel" is used when referring to a set of specified quantum numbers describing the reaction. A nuclear reaction progresses from the entrance channel, where the initial particles interact to various exit channels representing the different possible outcomes or final states of the reaction [32].

To investigate the structure of nuclear matter, nuclei, and nucleons, researchers conduct nuclear reactions. Elastic scattering of electrons and nucleons provides valuable information about the charge and mass distributions of nuclei. Nuclear states can be excited through inelastic scattering of particles, as well as through transfer and knock-out reactions, collectively referred to as direct reactions. When an excited intermediate nuclear system is formed, living up to 10^{-15} seconds and subsequently decaying with particle and γ-ray emissions, the reaction is termed a compound nucleus reaction. In the realm of nuclear reactions, new nuclei, such as exotic nuclei located far outside the line of highest stability (e.g. ^{16}C), or super heavy nuclei with charge numbers $Z \geq 100$, can be produced using heavy ion reactions. Researchers are presently exploring the transition of hadronic matter into aquark-gluon plasma through reactions involving highly relativistic heavy ions. This brief overview underscores the interconnectedness of nuclear reaction theory with the theory of nuclear structure and various nuclear models [32, 33].

2.2. Types of nuclear reaction

Nuclear Reaction can be subdivided according to time scales or, equivalently, the number of intra nuclear collisions taking place before emission. Light particle induced nuclear reaction above 10MeV can be categorized as (i) direct reaction. (ii) Pre equilibrium reactions. (iii) Equilibrium reaction.

2.2.1. Direct reaction

A direct response occurs when the projectile predominantly engages with the nucleons on the surface of the target nucleus. This interaction involves one or two nucleons, resulting in minimal energy and momentum transfer to only a few nucleons. The emitted particle is most likely directed along the projectile's motion. Direct reactions, also known as peripheral processes, represent the opposite extreme of compound-nucleus reactions, emphasizing surface interactions with the target nucleus. As the incident particle's energy increases, its de Broglie wavelength decreases, making it more probable to interact with a nucleon-sized object rather than a nucleus-sized one [34].

A reaction earns the designation "direct" when it smoothly progresses from the initial to the final state without the formation of an intermediate compound nucleus, involving in one or a few steps. In contrast, direct reactions are characterized by their speed, while compound reactions emerge at a slower pace. The challenge lies in defining the terms "a few," "fast," and "slow." The time scale provides a tangible measure, comparing the reaction speed to the motion of nucleons within the nucleus.

To contextualize this, a nucleon typically takes approximately 10^{-22} seconds to orbit a nucleus. If a reaction occurs within this time scale or even faster, it is categorized as a direct reaction. On the contrary, the formation of a compound nucleus necessitates a much more prolonged interaction [35].

As the projectile undergoes successive interactions, it progressively penetrates the target more deeply, ultimately leading to the formation of a compound nucleus. However, the reaction has the potential to conclude after only a few interactions, without reaching the stage of compound nucleus formation [36]. Ultimately, direct reactions often occur peripherally, meaning they take place at the nuclear surface. However, this generalization may not always hold true, as the nucleus can be nearly transparent to incident nucleons. In such cases, direct reactions involving neutrons and protons as projectiles can take place inside the nucleus rather than solely at the surface.

2.2.2. Pre equilibrium reaction

A pre-equilibrium reaction stands apart from both direct reactions and compound nucleus reactions. In these reactions, particles are emitted subsequent to the initial stage of a nuclear interaction (direct reaction), occurring well before the establishment of statistical equilibrium associated with compound nucleus formation.

The time scale of pre-equilibrium reactions falls in between the rapid direct reactions and the comparatively slow process of compound nucleus formation. Within pre-equilibrium reactions, particle emission from the excited target nucleus does not result from the statistical decay of the compound nucleus or immediate emission after the collision. Instead, the projectile imparts its energy to a limited number of nucleons within the target. Struck nucleons initiate a cascade of reactions with the target, during which a particle may be emitted before the compound nucleus reaches a state of statistical equilibrium. The projectile's energy is distributed among the target's nucleons through a cascade of nucleon interactions, exciting particle-hole states progressively [28].

A pre-equilibrium reaction involves the emission of an unbound particle from one of these particle-hole states when the composite nucleus has not yet equilibrated. Most pre-equilibrium reactions occur at energies high enough to render the resolution of individual final states impractical. The cross-sections in these cases pertain to reactions with a continuum of final states.

The absence of fluctuations in these continuum spectra suggests a high degree of accuracy in assuming no interference effects. Consequently, pre-equilibrium cross-sections can be assessed by adding the contributions from each stage of the nucleon-nucleon interaction cascade incoherently. The total cross-section for pre-equilibrium emission is then the sum of the cross-sections for emission from each stage of the cascade. In reactions occurring before reaching statistical equilibrium, the nuclear complex undergoes breakup prior to full equilibration. These reactions can be explained using a time-dependent framework, where the dynamics of populating and depopulating various configuration classes are governed by master equations.

2.2.3. Pre-equilibrium Models

The pre-equilibrium models became rather popular tool to analyse and understand nuclear reactions at excitation energies ranging from several tens of MeV up to the GeV regions. These quantum mechanical models provide, in principle, way of calculating the cross-sections of pre-equilibrium processes without the uncertainties of the semi-classical approximations [28]. There are different types of pre-compound nuclear reaction models.

2.2.3.1. Hybrid model

The hybrid model in nuclear reactions is a theoretical framework designed to describe various aspects of nuclear reactions, particularly at intermediate to high energies. This model combines features from different theoretical models to offer a more comprehensive understanding of the dynamics and outcomes of nuclear collisions. It encompasses Intra nuclear Cascade Model in which the initial phase of the model where incident particles (like protons, neutrons, or other hadrons) collide with nucleons (protons and neutrons within the nucleus). These collisions can lead to further interactions as struck nucleons can in turn interact with other nucleons in the nucleus, creating a cascade effect. The INC effectively models the high-energy part of a nuclear reaction where particle interactions and energy transfers occur rapidly [37].

This model combines various theoretical approaches to provide a comprehensive description of the nuclear reaction processes, which includes intra nuclear cascade, pre-equilibrium dynamics, and equilibrium decay. Each phase of the reaction is handled by different theoretical models that are best suited to describe the specific dynamics occurring at that stage. The hybrid model is particularly useful in scenarios involving intermediate and high-energy nuclear reactions where multiple phases of interaction occur. It's employed in nuclear physics research to understand fundamental interactions and the properties of nuclear matter, astrophysical contexts where nuclear reactions under extreme conditions need to be modeled.

The hybrid model in nuclear reactions is a robust framework that integrates various aspects of nuclear reaction theory to address the complex phenomena observed in nuclear interactions, particularly at higher energies. It allows researchers and engineers to predict the outcomes of nuclear reactions more accurately by acknowledging the different stages and dynamics involved in such processes [38].

2.2.3.2. Geometry Dependent Hybrid Model

In a geometry-dependent hybrid model, the distribution of the nucleon density in the target nucleus can affect the pre-equilibrium decay. This model describes the HMB and exciton model combinations. It considers the geometry effects and assumes the reduced matter density. In this model, multi-pre-equilibrium particle emission along with equilibrium decay is considered, and the spectra of the emitted particles are calculated for each step in the energy dissipation process induced by the interaction between the projectile and target nucleus [39].

Blann first put forward a commonly used hybrid H model for the description of the pre-compound (PC) reaction mechanism [40]. According to Blann, the PC differential reaction cross section can be calculated as follows:

$$\frac{d\sigma_v(\Sigma)}{d\Sigma} \sigma_{RP_v}(\Sigma) \qquad (2.7)$$

Here, σ_R represents the reaction cross section, and the term $P_V(\Sigma)$ represents the number of particles of the type emitted into the unbounded continuum with channel energy between ε and ε +dε. For many years, the geometry-dependent hybrid (GDH) model has been reasonably successful in reproducing a broad range of data [41]. The GDH model is an advanced and modified form of the H model in which the nuclear geometry effects and the reduced matter density are considered, which sustained a shallow potential. Thus, the diffused surface properties of higher impact parameters were incorporated into the PC emission formalism in the GDH model.

As a result, the differential reaction cross section for PC emission in the GDH model is formulated as:

$$\frac{d\sigma_v(\Sigma)}{d\Sigma} = \pi\lambda^2 \sum_{l=0}^{\infty}(2l + 1)\, T_l P_v(l, \Sigma) \qquad (2.8)$$

T_l represents the transmission coefficient for the l^{th} partial wave, and the quantity $P_v(l, \Sigma)$ represents decay probability at 'ε' channel energy and 'l' orbital angular momentum. 'λ' is the reduced de-Broglie wavelength.

2.2.3.3. Exciton Model

Exciton model is presented by Griffin and is logically simple and modified. In this model, the incoming projectile interacting with the target nucleus gives rise to a simple initial configuration characterized by a small number of excited particles and holes called excitons [25]. The nuclear state is characterized by the excitation energy of the composite nucleus and the exciton number, which is the total number of particles (p) above and holes (h) below the Fermi surface. Successive two -body interactions increase the number of excitons and lead to a fully equilibrated residual nucleus. Griffin introduced two basic hypotheses to describe each stage of composite nucleus.

1. At each state of the cascade all the state with the same configurations and the same total energy are equiprobable.

2. At each state of the cascade all the processes which may occur are equiprobable.

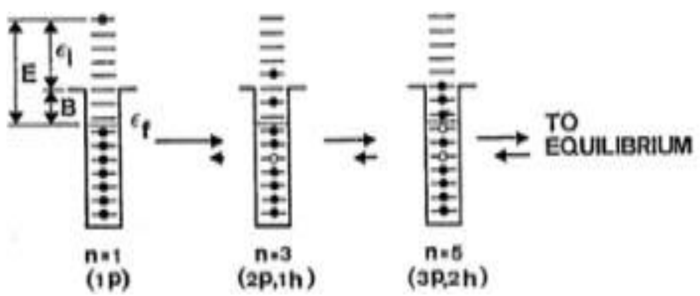

Figure.2.2. Representation of the equilibration process as formulated in the exciton model [26].

The symbols as indicated in Figure. 2.2. Represent: - E = Excitation energy, B = binding energy

n= number of exciton, o = hole □ = particle Σ_f = Fermi energy

Since all the levels below the Fermi energy are filled, the first projectile-target interaction brings two particle-one hole (2p+ 1h) state which produces a total exciton number of 3; i.e. n = p + h = 3 , the next interaction may be (3p, 2h) state, i.e. n = p + h = 5 and so on. In this cascade interactions, $\Delta p = 0, \pm 1$ and $\Delta h = 0, \pm 1$; then $\Delta n = 0, \pm 2$. The pre-equilibrium exciton model is governed by the set of master equation which describes both competing processes the equilibrium of the nucleus and the emission. In the simple case, when we consider just one possible excitation energy and only the composite system prior to and including the first emission, this set reads [25].

2.2.3. Compound Reaction

Niels Bohr introduced the concept of a fully equilibrated "compound" nuclear system in 1937. In this model, the decay of the system is independent of how it was originally formed [26]. The statistical model employed in EMPIRE represents an advanced implementation of the Hauser-Feshbach theory. It meticulously incorporates the exact angular momentum and parity coupling. The model accounts for the emission of various particles, including neutrons, protons, α-particles, deuterons, tritons, and He-3. Additionally, it considers the competing fission channel. Bohr categorized the reaction as a two-step process within this framework [42].

Formation of compound nucleus

Formation of a compound nucleus is a reaction where two nuclei merge to create a single, excited nucleus. This excited state persists for a comparatively extended period, during which it essentially "forgets" its origin. The subsequent decay from this excited state occurs through the process of "evaporation," involving the expulsion of nucleons from the heated liquid drop of the compound nucleus. Alternatively, decay can take place through gamma decay or by the fission of the compound nucleus. The statistical nature of this decay process provides insights into the average properties of excited states in complex nuclei. It highlights the random and probabilistic aspects of the interactions with in the compound nucleus, shedding light on the behavior and characteristics of such intricate nuclear systems [4]. The creation of a compound nucleus is a gradual process, taking on the order of seconds, in contrast to the brief period for a typical nucleon projectile, which lasts only a few MeV. This brief duration, referred to as nuclear time, typically ranges from 10^{-21} to 10^{-22} seconds. As the compound nucleus forms, there is a transfer of energy and momentum during interactions between the incoming projectile and the nucleons within the target. This exchange is distributed across the entire nucleus over the considerable time span.

In the course of numerous collisions between nucleons, a state of static thermodynamic equilibrium is eventually reached. At this point, it becomes challenging to distinguish the projectile nucleon from others. The compound nucleus essentially loses memory of its formation process. When a projectile, denoted as "a," interacts with a target nucleus X, it penetrates the target and establishes a new system:

$$\mathrm{a} + \mathrm{X} \rightarrow \mathrm{C}^{*} \qquad (2.9)$$

Here, C* represents a compound system in an excited state.

The duration of this process is significant enough for the resulting C* system to forget its origin, meaning it no longer retains information about the projectile (a) or the target (X). For instance, the compound nucleus $^{27}_{13}$Al* can be formed through various reaction processes:

$^{4}_{2}$He(α)+$^{23}_{11}$Na → $^{27}_{13}$Al* (α-as a projectile)

$^{1}_{1}$H(p) + $^{26}_{12}$Mg → $^{27}_{13}$Al* (proton as a projectile)

$^{1}_{0}$n + $^{26}_{13}$Al → $^{27}_{13}$Al* (neutron as a projectile)

Regardless of the specific reaction pathway, the compound nucleus is produced through the incoming channel (a + x), and once formed, it essentially erases any memory of the initial projectile or target [1].

Decay of Compound Nucleus

Owing to the forgetfulness inherent in the compound nucleus, its decay process is distinct and unrelated to its formation. The mechanism of decay relies solely on the excitation energy of the compound nucleus and is independent of the specific pathway through which it was created. Generally, the Compound Nucleus model is most effective at lower energies, typically in the range of 10 to 20 MeV. In this energy range, the incident projectile has a limited probability of escaping the nucleus while retaining its identity and a significant portion of its energy is absorbed through interactions. This model is particularly well-suited for medium-weight and heavy nuclei, where the size of the nuclear interior is sufficient to absorb the incident energy.

Another characteristic of compound nucleus reactions is the angular distribution of the resulting products. Due to the stochastic nature of interactions among nucleons, the outgoing particles are expected to be emitted with nearly isotropic angular momentum. When a heavy ion serves as the incident particle, substantial angular momentum can be transferred to the compound nucleus. To release this angular momentum, the emitted particles tend to be preferentially emitted at right angles, corresponding to 0 and 180 degrees in the angular distribution [26]. With light projectiles, this phenomenon is insignificant. The analogy to evaporation, as mentioned earlier, remains highly relevant. Essentially, the greater the energy supplied to the nucleus, the higher the probability of particle evaporation. In the case of light projectiles, this effect is minimal.

The analogy to evaporation, as emphasized earlier, holds true, underscoring that as we increase the energy input to the nucleus, the probability of particle evaporation also rises.

In 1950 the first experiment was done in USA by an Indian S.N.GHOSLAL [45]. In the experiment two projectiles such as α particle and proton were selected to make compound nucleus of $^{64}Zn^*$. For alpha-particle the target was $^{60}_{28}Ni$ and for the proton target was $^{63}_{29}Cu$ is selected [26].

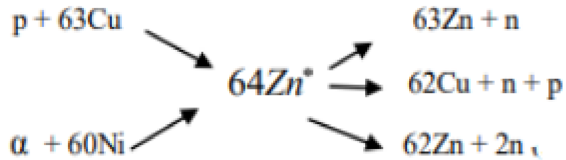

(2.10)

When the idea of the compound nucleus is valid and if one chooses the energy of the proton and the incident α-particle to produce the same excitation energy then the cross section for each one of the three exit channels should be independent of the way the compound nucleus is formed. This is the properties of the compound nucleus do not have any relationship with the nuclei that forms it. According to Bohr theory, we can write the cross-section of formation of compound nucleus $\sigma_c(a)$, the probability of disintegration of compound nucleus Y and emitted particle 'y' of a nuclear reaction X(a, b)Y in the form

$$\sigma(a, b) = \sigma_c(a) G_c(b) \qquad (2.11)$$

Where $\sigma_c(a)$ is the cross - section for the formation of compound system by the particle 'a' incident up on the target nucleus X and G_C (b) is the probability that the compound system C once formed, decays by emission of particle 'b' leaving a residual nucleus Y. It is assumed that G_C (b) is a pure number independent of the mode of formation of the compound nucleus.

In a more reasonable way, if the sum is extended over all particles b which c can emit, it can be expressed as [44].

$$\sum_b G_c(b) = 1 \qquad (2.12)$$

It is more important to specify the reaction X(a, b)Y in greater detail in terms of the cross section σ(α, β) corresponding to a specific entrance channel (α) and exit channels (β) as follows:

$$\sigma(\alpha, \beta) = \sigma_c(\alpha) G_c(\beta) \qquad (2.13)$$

Due to Bohr assumption, the decay of the compound system in to the different channels β, Y etc, depends only on the energy E_C, the angular momentum J_C, and the parity of the compound system. In order to simplify our present consideration the dependence properties of the compound system on the angular momentum J_C and the parity will be ignored in this section[25].

Now introduce a few magnitudes which describe the disintegration of the compound system. We begin with the mean life time τ (E_C) of C before decay and define the magnitude

$$\Gamma\,(E_c) = \frac{\hbar}{\tau E_C} \qquad (2.14)$$

Which is ħ times the rate of disintegration per unit time. Γ is energy and, later on, will play the role of a level width.

We can therefore call it the total width of the state of C with excitation energy E_C. C can decay in to various channels and its total decay rate Γ can be subdivided in to decay rates referring to specific channels [25].

$$\Gamma\,(E_c) = \sum_{\beta} \Gamma_{\beta}(E_c) \qquad (2.15)$$

Where the sum is extended over all channels in to which C can decay, i.e., over all open channels. The specific decay rate is also Γ (E_C) a function of Σ_C and is called the partial width for the decay in to channel β. The magnitude Γ_β can also be defined as follow:

If an assembly of N equal samples of the compound system C is arranged in such a way that, on the average N system constant in time (i.e. as many compound systems decay are produced) then the number of decays in to channel β per unit time is given by

$$\frac{N\Gamma_{\beta}}{\hbar} \qquad (2.16)$$

We can now express the branching probability in terms of the decay rates by the reaction

$$G_c(\beta) = \frac{\Gamma_{\beta}}{\Gamma} \qquad (2.17)$$

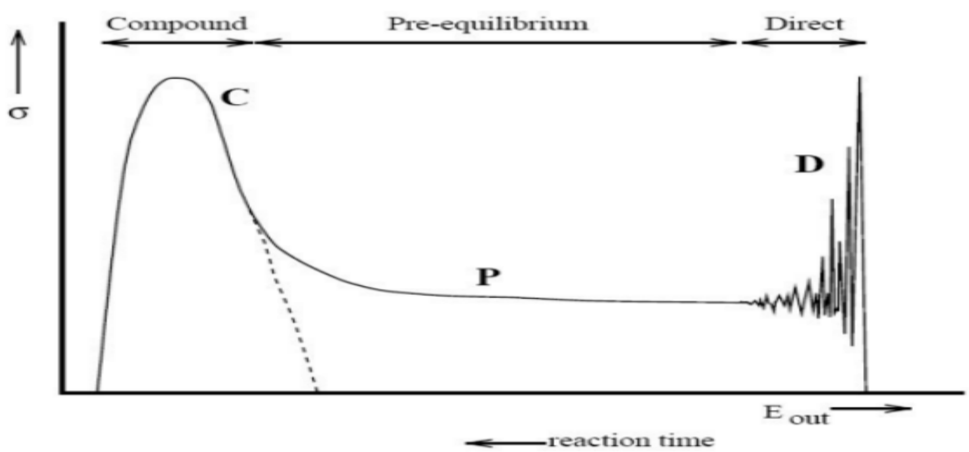

Figure 2.3 Schematic drawing of nuclear reaction [25].

2.2.4. Compound Nucleus Models

Nuclear reactions calculations based on standard nuclear reaction models play an important role in determining the accuracy of various parameters of theoretical models and experimental measurements. Especially, the calculations of nuclear level density parameters for the isotopes can be helpful in the investigation of reaction cross-sections [45]. There are several nuclear reaction model codes available to simulate compound nucleus reaction and decay process [46]. The nuclear level density is the main ingredients for statistical characteristics of excited nuclei, EMPIRE and TALYS incorporated different level density models to calculate cross-sections.

2.2.4.1. Fermi-Gas Model

Fermi-Gas description is widely applied in the recent versions of most of the computer codes for nuclear reaction calculations [47]. The density of intrinsic levels with spins J, parity π and excitation energy E_x is factorized in terms of state density and spin and parity dependence as [42].

$$\rho E_x\,(J, \pi) = \rho\,(E_x)\,\rho\,(J, \pi) \tag{2.18}$$

The energy dependence reads

$$\rho E_x = \frac{\exp S}{\sqrt{\mathrm{Det}}} \tag{2.19}$$

Where S is the entropy and Det is defined by eq. (2.21)

The spin and parity dependence is given by

$$\rho\,(J, \pi) = \frac{1}{2}\frac{2J+1}{\sqrt{8\,\pi\,\sigma^3}}\exp\left[\frac{\left(J+\frac{1}{2}\right)^2}{2\sigma^2}\right] \tag{2.20}$$

Where σ^2 the spin cut-off parameter and equal parity distribution is assumed. For the Fermi-Gas model the state equations determining the dependence of the excitation energy, entropy and other thermodynamic functions of a nucleus on its temperature T are.

$$E_x = aT^2;\ S = 2aT;\ \sigma^2 = \Im T;\ \mathrm{Det} = 144a^3\,\frac{T^5}{\pi} \tag{2.21}$$

Where a, is the level density parameter and $\Im$ is the nuclear moment of inertia. To account for the odd-even ejects in nuclei, the excitation energy is replaced in calculations with the ejective energy.

$$U = E_x - \Delta \tag{2.22}$$

Where, Δ is equal or closely related to the pairing energy. The well-known expression for the state density is

$$\rho^{FG}(E_X) = \frac{\sqrt{\pi}}{12a^{\frac{1}{4}}U^{\frac{5}{4}}} \exp(2\sqrt{aU}) \qquad (2.23)$$

$$\rho^{FG}(E_{X,} J, \pi) = \frac{2J+1}{48\sqrt{2}\, U^{\frac{5}{4}}\, \sigma^{\frac{3}{2}}\, a^{\frac{1}{4}}} \exp\left[2\sqrt{aU} - \frac{\left(J+\frac{1}{2}\right)^2}{2\sigma^2}\right] \qquad (2.24)$$

These equations show that nuclear level densities in Fermi-Gas model depend on three parameters: a, σ and Δ

2.2.4.2. Generalized Super Fluid Model

Generalized Super fluid Model is a default model used in EMPIRE-3.2 code to adjusted discrete levels and level density retrieved from reference input parameter library (RIPL- 2). This model use constant temperature model below critical energy and Fermi gas model above critical energy depend on the compound nucleus excitation energy. The phenomenological model is characterized by a phase transition of superfluid behaviour at low energy where the level density is strongly influenced by pairing energy term. The generalized super fluid model distinguishes between a low and high energy region [40]. The level density for the generalized super fluid model has been calculated as follows [48].

$$\rho\,(U) = \rho_{qp}U^1 K_{vib}(U^1)\, K_{rot}(U^1) \qquad (2.25)$$

Where the term ρqpU^1 denotes the density for quasi particle nuclear excitation and the terms $K_{vib}(U^1)$ and $K_{rot}(U^1)$ represent rotational and vibrational enhancement factors at the U^1 effective energy of excitation.

2.2.4.3. Enhanced Generalized Super Fluid Model

Enhanced Generalized Super fluid Model is a default model used in EMPIRE-3.2 code to adjusted discrete levels and level density retrieved from reference input parameter library (RIPL-3).The RIPL-3 includes the nuclear masses, discrete levels and decay schemes, neutron resonances, optical model parameters, level densities, gamma-ray strength function and fission barriers [40]. The model uses the super-fluid model below critical excitation energy and the Fermi gas model at energy above it. In non-adiabatic approximation, collective enhancements due to nuclear vibration and rotation are taking into account [46]. Hence it considers the shape of the nucleus in the dynamical situation.

This deformation enters level densities formulas through moments of inertia and through the level density parameter that increases with increase in the surface of the nucleus.

2.2.4.4 Optical Model

When a nuclear reaction takes place the two nuclei combine together, and in this system, a single nucleon is in the field created by all the remaining nucleons. If we have ‘n’ number of nucleons in a system then ‘n’ number of Schrodinger’s equations are required to represent the system. It is necessary to have the appropriate form of potential in order to solve the equations. In the optical model, this potential is considered complex, which has a real part as well as an imaginary part.

The interaction between the incident particle and the nucleus is considered as an optical phenomenon. As an electromagnetic wave enters one media to another media, it may get refracted and when some obstacle is in the path it may get diffracted. In the same manner, the incident particle wave is diffracted by the nucleus. Hence the overall potential V(r) contains a real part representing the diffraction phenomenon and imaginary part representing the refraction part. The potential is represented by the following equation, with real part U(r) and imaginary part jW(r).

$$V(r) = U(r) + jW(r) \qquad (2.26)$$

An essential value of good optical model is reliable prediction of the quantities for energies and nuclides for which no measurement exists and also the impact on the evaluation of the various channels; such as transmission coefficients for compound nucleus and pre-equilibrium model including the distorted wave functions that are used for direct inelastic reactions and for transitions to the continuum that describe statistical multi-step direct reactions. The Phenomenological optical [46] model potential for incident neutrons and protons is defined as:

$$V(r) = V_C(r) + Uf_s(r) + iW_g(r) + \left(\frac{\hbar^2}{m_x c}\right)^2 \frac{1}{r} U_S \frac{df_S}{dr} 1.S \qquad (2.27)$$

Where $V_C(r)$ is the electrostatic potential of the nucleus included only in the proton optical Potential. U, W and U_s are respectively real, imaginary and spin-orbit potential depths. The quantity l.S represents the scalar product of the intrinsic and orbital angular momentum operation and is given as;

$$l.S = l \text{ for } j = l + \frac{1}{2} \qquad (2.28)$$

$$l.S = -(l+1) \text{ for } j = l - \frac{1}{2} \qquad (2.29)$$

Due to the short-range interaction of nucleon-nucleon, the potential $Uf_s(r)$ which is approximately the sum of nucleon interactions has the same behaviors. The nucleons in the core of the nucleus undergo only the interaction with the closet neighbors. Due to this saturation of the nuclear forces, the potential $Uf_s(r)$ is uniform inside the nucleus and then decrease exponentially in the surface region. The variation of the real part of the interaction potential is approximated by a Wood-Saxon function:-

$$f_s(r) = \frac{1}{1+\exp\left[\frac{r- R_i}{a_i}\right]} \qquad (2.30)$$

Where the geometry parameters are the radius $R_i = r_i A^{\frac{1}{3}}$ with A the atomic mass number, the diffuseness a_i for each component. The form factor g_r is derived function of Woods-Saxon situated at the surface of the nucleus:

$$g_r = 4a\,\frac{df(r)}{dr} \qquad (2.31)$$

When complex nuclear potential is introduced in the radial part of Schrödinger equation, the total elastic scattering is defined as

$$\sigma_T = \sigma_T + \sigma_E \qquad (2.32)$$

Optical model helps to separate the incident projectile flux into three main components. Such as shape elastic, the direct elastic and reaction cross section and it also serves as a basis for evaluation process by providing neutron transmission coefficient used in Hauser-Feshbach theory for nuclear evaluation.

2.3. Nuclear Reaction cross section

The reaction cross-section stands out as a fundamental parameter in the examination of nuclear reactions [17]. When a target encounters the impact of a projectile, an interaction unfolds, involving a specific number of nuclei. This participation can vary, with nuclei engagement in the reaction categorized as either limited or extensive. This numerical factor significantly influences the probability of a specific reaction taking place. To quantify this probability, the concept of reaction cross-section becomes a pivotal measure. In an illustrative scenario, imagine an experiment where a thin slab of target material is exposed to a mono-energetic beam comprising uniformly distributed particles over a specific area. If the nuclear reaction yields particles within a given timeframe, an associated area perpendicular to the incident beam is conceptualized for each target nucleus.

If the center of the bombarding particle strikes within this area, a reaction occurs; otherwise, no reaction takes place. This hypothetical area, denoted as σ (cross-section), provides a measure of the reaction probability per target nucleus. Notably, this imaginary area doesn't necessarily correspond to the cross-sectional area (πr^2) of the impacted nucleus.

The likelihood of a reaction can alternatively be expressed through the ratio $\frac{N}{I}$; however, it's important to note that this quantity depends on both the target density and its thickness (Δx). In contrast, σ is specifically linked to an individual target nucleus, offering a more focused measure of the reaction probability per nucleus [28]. The probability of a successful hit $\frac{N}{I}$ for any individual bombarding particle is equivalent to the projected total cross-section of all target nuclei positioned within the area A, as observed along the beam direction, divided by A. In a scenario where there are target nuclei per unit volume represented by $nA\Delta x$ in the target material, these nuclei are within the potential reach of any bombarding particle in the beam.

Each of these target nuclei is associated with a cross-section, allowing the total reaction probability for the entire volume to be expressed as $\sigma = nA\Delta x$.

$$\frac{N}{I} = \frac{nA\Delta x\sigma}{A} \tag{2.33}$$

Using this relation we can define cross-section by writing [28]

$$\sigma = \frac{N}{\frac{I}{A}nA\Delta x} \tag{2.34}$$

Experimentally cross-section is measured by the ratio

$$\sigma = \frac{\text{number of reaction per second per nucleus}}{\text{number of projectiles incidet per second per unit area}} \tag{2.35}$$

The concept of a nuclear cross section can be quantified physically in terms of "characteristic area" where a larger area means a larger probability of interaction. The standard unit for measuring a nuclear cross section (denoted as σ) is the barn, which is equal to 10^{-28} m^2, 10^{-24} cm^2 or 100 fm^2. Cross sections can be measured for all possible interaction processes together, in which case they are called total cross section, or for specific processes, distinguishing elastic scattering and inelastic scattering ; of the latter, amongst neutron cross section, the absorption cross section are of particular interest [38].

2.4. Partial Wave Analysis

Nuclear reaction cross-section may be explained using wave mechanical theory under general assumptions [48]. Let us consider a collimated beam of neutrons taking on the target, the beam is moving in Z-direction. This neutron beam can be considered as a plane wave exp(ikz) [48, 3].

$$\psi_{inc} = e^{ikz} \quad (2.36)$$

The plane wave can be explained in terms of Bessel's functions and spherical harmonic of various values of ℓ.

$$e^{ikz} = \sum_{\ell=0}^{\infty} i^{\ell}\,(2\ell+1) j_\ell(kr) p_\ell(\cos\theta) \quad (2.37)$$

$$j_\ell(kr) = \frac{\sin(Kr - \frac{\ell\pi}{2})}{kr} \quad (238)$$

$$p_\ell(\cos\theta) = \sqrt{\frac{4\pi}{2\ell+1}}\, Y_{\ell 0}(\theta) \quad (2.39)$$

For r→ ∞ then the Bessel function $j_\ell(kr) = \frac{\sin(kr - \frac{\ell\pi}{2}}{kr}$

$$e^{ikz} = \psi_{inc} \quad (2.40)$$

$$\psi_{inc} = \frac{1}{kr} \sum_{l=0}^{\infty} i^{\ell}\,(2\ell+1)\sin(kr - \frac{\ell\pi}{2} p_\ell(\cos\theta) \quad (2.41)$$

$$\psi_{inc} = \frac{1}{2ikr} \sum_{\ell=0}^{\infty} i^{\ell}(2\ell+1)[e^{i\left(kr - \frac{\ell\pi}{2}\right)} - e^{-i(kr - \frac{\ell\pi}{2})}\,]p_\ell(\cos\theta) \quad (2.42)$$

$$\psi_{inc} = \frac{1}{2kr} \sum_{\ell=0}^{\infty} (2\ell+1) i^{\ell+1} \left[e^{-i\left(kr - \frac{\ell\pi}{2}\right)} - e^{i\left(kr - \frac{\ell\pi}{2}\right)}\right] p_\ell\,(\cos\theta) \quad (2.43)$$

The first term $e^{-i\left(kr - \frac{\ell\pi}{2}\right)}$ in going wave and the second term $e^{i\left(kr - \frac{\ell\pi}{2}\right)}$ outgoing wave.in the presence of a nucleus the amplitude of outgoing wave is modified.

$$\psi(r) = \frac{1}{2kr} \sum_{\ell=0}^{\infty} (2\ell+1) i^{\ell+1} \left[e^{-i\left(kr - \frac{\ell\pi}{2}\right)} - \eta_\ell e^{i\left(kr - \frac{\ell\pi}{2}\right)}\right] p_\ell\,(\cos\theta) \quad (2.44)$$

$\eta_\ell = |\eta_\ell| e^{i\delta_\ell}$ Where $e^{i\delta_\ell}$ represents phase and $|\eta_\ell|$ is the amplitude.

If $|\eta_\ell|$ is changing, it means amplitude is decreasing, reaction is taking place. If δ_ℓ is changing then scattering is taking place.

If $|\eta_\ell|$ is not changing, it means no attenuation of amplitude and hence no reaction. If the phase is changing (phase shift) then scattering is taking place.

The scattered wave can be written as

$$\psi_{sc} = \psi(r) - e^{ikz} \qquad (2.45)$$

$$\psi_{sc} = \sum_{\ell=0}^{\infty} \frac{1}{2kr}(2\ell+1)i^{\ell+1}1 - \eta_{\ell}(e^{i\left(kr-\frac{\ell\pi}{2}\right)})p_{\ell}(\cos\theta) \qquad (2.46)$$

The scattered wave can be also written in terms of scattering amplitude as follows.

$$\psi_{sc} = f(\theta)\frac{e^{kr}}{r} \qquad (2.47)$$

$f(\theta)$ Is the scattering amplitude, then to get the value of $f(\theta)$ simply compare the above two equations

$$f(\theta)\frac{e^{kr}}{r} = \sum_{\ell=0}^{\infty} \frac{1}{2kr}(2\ell+1)i^{\ell+1}1 - \eta_{\ell}(e^{i\left(kr-\frac{\ell\pi}{2}\right)})p_{\ell}(\cos\theta) \qquad (2.48)$$

$$f(\theta) = \sum_{\ell=0}^{\infty} \frac{i^{\ell+1}}{2kr}(2\ell+1)e^{\frac{-i\ell\pi}{2}}(1-\eta_{\ell})p_{\ell}(\cos\theta) \qquad (2.49)$$

For any value of ℓ, $i^{\ell}\, e^{\frac{-i\ell\pi}{2}} = 1$, then the above equation becomes

$$f(\theta) = \frac{1}{2kr}\sum_{\ell=0}^{\infty}(1-\eta_{\ell})p_{\ell}(\cos\theta)(2\ell+1) \qquad (2.50)$$

To get the scattering cross-section, we consider a sphere of radius r_0 enclosing the scatterer. The values of r_0 are very much larger than the nuclear force range. The number of scattered particle through the solid angle $d\Omega$ is equal to the number of particles scattered through $r_0^2\, d\Omega$. N_{sc} Can be calculated using the expression of the probability of current density,

$$N_{sc}=\frac{\hbar}{2mi}\int\left(\frac{d\psi_{sc}}{dr}\psi_{sc}^{*} - \frac{d\psi_{sc}^{*}}{dr}\psi_{sc}\right)_{r=r_0}^{r_0^2\sin\theta d\theta d\varphi} \qquad (2.51)$$

Where $k=\frac{\sqrt{2mE}}{\hbar}$ hence $\frac{\hbar k}{m}=\frac{\hbar\sqrt{2mE}}{\hbar m}=\frac{\sqrt{2mE}}{m}$ and $v=\frac{\sqrt{2E}}{\sqrt{m}}=\frac{\sqrt{2mE}}{m}$

The above equation becomes,

$$N_{sc}=\frac{\hbar k}{m}\int |f(\theta)|^2\sin\theta d\theta d\varphi \qquad (2.52)$$

Where m is the mass number of incident particle

$$N_{sc} = V\int |f(\theta)|^2 d\Omega \qquad (2.53)$$

$$N_{sc} = \frac{v\pi}{k^2}\sum_{l=0}^{\infty}(2\ell+1)(1-|\eta_{\ell}|^2) \qquad (2.54)$$

Due to orthogonally a normalization of spherical harmonics and Legendre polynomial.

$$p_\ell(\cos\theta) = \sqrt{\frac{4\pi}{2\ell+1}}\, Y_{\ell m} \tag{2.55}$$

$$\sigma_{sc} = \frac{N_{sc}}{\text{Incdent flux}} \tag{2.56}$$

Incident flux for a plane wave e^{ikz} moving with velocity v

$$\int \psi\psi^* d\tau = 1 \tag{2.57}$$

Particle density in a plane wave is the flux of plane wave number of particle per second per unit area=v then,

$$\sigma_{sc} = \frac{N_{sc}}{\text{Incdent flux}} \tag{2.58}$$

$$\sigma_{sc} = \frac{N_{sc}}{v} = \frac{\pi}{k^2} \sum_{\ell=0}^{\infty} (2\ell+1)(1-|\eta_\ell|^2) \tag{2.59}$$

Where, from the relation $P = \frac{\hbar}{\lambda} = \hbar k$

$$\sigma_{sc} = \pi\lambda^2 \sum_{\ell=0}^{\infty} (2\ell+1)(1-|\eta_\ell|^2) \tag{2.60}$$

$$\sigma_{sc} = \pi\lambda^2 (2\ell+1)(1-|\eta_\ell|^2) \tag{2.61}$$

Then let calculate the reaction cross-section using the probability current density expression. Now first let calculate number of particles going in

$$N_r = -\int\int \frac{\hbar}{2mi}\left(\frac{d\psi_r}{dr}\psi_r^* - \frac{d\psi_r^*}{dr}\psi_r\right) r_0^2 \sin\theta d\theta d\varphi \tag{2.62}$$

In place of ψ_{sc} we have ψ_r

$$N_r = \frac{\hbar\pi}{mk} \sum_{\ell=0}^{\infty} (2\ell+1)\,(1-|\eta_\ell|^2) \tag{2.63}$$

$$\sigma_r = \frac{N_r}{\text{Incdent flux}} = \frac{N_r}{v} \tag{2.64}$$

$$\sigma_r = \sum_{\ell=0}^{\infty} \sigma_{r,\ell} = \frac{\pi}{k^2} \sum_{\ell=0}^{\infty} (2\ell+1)(1-|\eta_\ell|^2) \tag{2.65}$$

$$\sigma_r = \pi\lambda^2 (2\ell+1)(1-|\eta_\ell|^2) \tag{2.66}$$

Then the total cross section $\sigma_{t,\ell}$ is given as

$$\sigma_{t,\ell} = \sigma_{sc,\ell} + \sigma_{r,\ell} \tag{2.67}$$

$$\sigma_{r,\ell} = \pi\lambda^2(2\ell + 1)[(1 - |\eta_\ell|^2) + |1 - \eta_\ell|^2] \tag{2.68}$$

$$\sigma_{t,\ell} = \pi\lambda^2(2\ell + 1)[(1 - \eta_\ell\eta_\ell^* + (1 - \eta_\ell)(1 - \eta_\ell^*)] \tag{2.69}$$

$$\sigma_{t,\ell} = \pi\lambda^2(2\ell + 1)[2 - \eta_\ell - \eta_\ell^*] \tag{2.70}$$

$$\sigma_{t,\ell} = \pi\lambda^2(2\ell + 1)[2 - (\mathrm{Re}\eta_\ell + \mathrm{Img}\eta_\ell)] \tag{2.71}$$

$$\sigma_{t,\ell} = \pi\lambda^2(2\ell + 1)[2 - 2\mathrm{Re}\eta_\ell] \tag{2.72}$$

$$\sigma_{t,\ell} = \pi\lambda^2(2\ell + 1)[1 - 2\mathrm{Re}\eta_\ell] \tag{2.73}$$

Total cross section is given by only $\mathrm{Re}\eta_\ell, \eta_\ell = |\eta_\ell|e^{2i\delta_\ell}$, if $|\eta_\ell|$=1, $\eta_\ell = e^{2i\delta_\ell} = \cos 2\delta_\ell + i\sin 2\delta_l$ then the real part of $\eta_\ell = \mathrm{Re}\eta_\ell = \cos 2\delta_\ell$, hence 1- $\mathrm{Re}\eta_\ell = 2\sin^2\delta_\ell$

$$\sigma_{t,\ell} = 2\pi\lambda^2(2\ell + 1)2\sin^2\delta_\ell \tag{2.74}$$

$$\sigma_{t,\ell} = 4\pi\lambda^2(2\ell + 1)\sin^2\delta_\ell \tag{2.75}$$

$$\sigma_{t,\ell} = \pi\lambda^2(2\ell + 1)|1 - \eta_\ell|^2 \tag{2.76}$$

$$\sigma_{sc,\ell} = \pi\lambda^2(2\ell + 1)|1 - \eta_\ell|^2 \tag{2.77}$$

For $\eta_\ell = 1$ then $\sigma_{sc,\ell} = 0$ for $\eta_\ell = -1$ $\sigma_{r,\ell} = 0$ $\sigma_{sc,\ell} = 4\pi\lambda^2(2\ell + 1)$, for$\eta_\ell = 0$ $\sigma_{r,\ell} = \sigma_{sc,\ell} = \pi\lambda^2(2\ell + 1)$ and for $|\eta_\ell|$=1 then $\sigma_{r,\ell} = 0$ $\sigma_{sc,\ell}$=finite

When reaction cross-section is zero, scattering is also zero, when reaction cross-section is maximum at ($\eta_l = 0$) scattering cross-section is equal to reaction cross-section and when scattering is maximum, reaction is zero. In fact, Reaction is zero when scattering is maximum Scattering is possible without reaction but no reaction is possible without scattering.

$$\sigma_{r,\ell} = \sum_{\ell=0}^{\infty} \pi\lambda^2(2\ell + 1)(1 - |\eta_\ell|^2) \tag{2.78}$$

$$\sigma_{r,max} = \sum_{\ell=0}^{\infty} \pi\lambda^2(2\ell + 1)\,|\eta_\ell| = 0 \tag{2.79}$$

$$\sigma_{sc} = \sum_{\ell=0}^{\infty} \pi\lambda^2(2\ell + 1)\,|\eta_\ell| = 0 \tag{2.80}$$

$$\sigma_{total} = \sigma_{r,max} + \sigma_{sc} = 2\pi\lambda^2 \sum_{\ell=0}^{\infty}(2\ell + 1) \tag{2.81}$$

$$\sigma_t = 2\pi\lambda^2(\ell_m + 1)^2 \tag{2.82}$$

Where $\ell_m = \frac{R}{\lambda}$

$$\sigma_t = 2\pi\lambda^2 \left(\frac{R}{\lambda} + 1\right)^2 = \sigma_t = 2\pi\lambda^2 \frac{(R+\lambda)^2}{\lambda^2} \tag{2.83}$$

$$\sigma_t = 2\pi(R + \lambda)^2 \tag{2.84}$$

For high energy R>> λ

$$\sigma_t = 2\pi R^2 \tag{2.85}$$

Total cross-section is twice of the geometrical cross-section of the nucleus. In the figure below, the vertical axis represents $\frac{\sigma_{sc,\ell}}{\pi\lambda^2(2\ell+1)^2}$and the horizontal axis represents $\frac{\sigma_{r.\ell}}{\pi\lambda^2(2\ell+1)^2}$

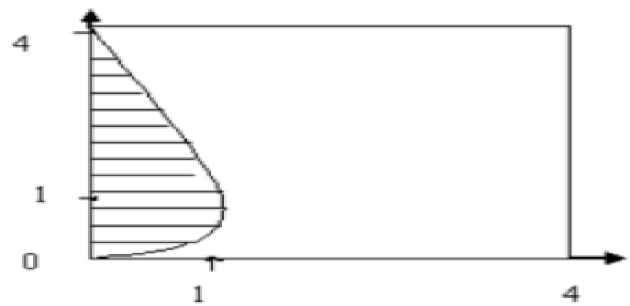

Fig.2.4 Possible values of scattering and reaction cross-section [3]

Chapter Three

Materials and Methods

Historically, various computer codes based on theoretical nuclear reaction models have been employed to anticipate cross-sections for the production of radionuclides. This study focuses on theoretical predicting the production cross-sections of medically used radionuclides, namely, ^{88}Y, ^{89}Zr ^{90}Y and ^{99}Mo. These radionuclides are expected to be generated through complex (α, n, x) channels in the interaction of α-projectiles with ^{89}Y, ^{96}Zr target at approximately 10 - 60 MeV of α-energies. The computer codes employed for these predictions include COMPLETE, TALYS-1.95(G), and EMPIRE-3.2

3.1. Computer codes

3.1.1. Complete code

Computer code COMPLET employed Weiss Kopf-Ewing model for the statistical component and Hybrid as well as geometry dependent hybrid model of Blann for PE emission. It is a modified and advanced computer code. This code has successfully predicted numerous nuclear data sets, particularly for the production of medical radionuclides [4]. It applies the statistical model of compound nucleus decay developed by Weiss Kopf- Ewing and the hybrid and geometric dependent model of Blann. In this code, three input parameters, namely: initial exciton number (n_o), level density parameter (a), and mean free path multiplier, were used in the theoretical predictions. The nuclear level density influences the shape and height of the calculated excitation functions. It was obtained by experiment and shows a linear dependence on the mass number of the compound nucleus. In general, it is given by an expression.

$$a = \frac{ACN}{K} \tag{3.1}$$

Where ACN is the mass of the compound nucleus and K is the free constant. In order to find the best-fitting value of K, the values of K are varied. The exciton number of the particles in the initial configuration is represented by n_o, which is described by the number of neutrons (n) and the number of protons (p) in excited states, and the number of holes (h) following the first interaction of a projectile with a target. A sensitive input parameter, n_o, is equal to the sum of n, p, and hole. To find the best fitted value n_o also vary too.

3.1.2. Empire-3.2 Code

EMPIRE-3.2 code is a modular nuclear reaction code comprising various nuclear models that predict cross sections for a broad range of energies and projectiles. The EMPIRE 3.2 Herman et al., [39], which uses the latest reference input parameter library RIPL-3 Capote et al., [40]. The codes were launched with the default input parameters, and all possible reaction channels were considered, including the emission of complex particles at our bombarding energies. The Enhanced Generalized Superfluid Model (EGSM) is a default level density model used in the present EMPIRE code calculations. This model was selected because it has been very successful in predicting the excitation function [39]. A projectile can be any neutron, proton, any ion (including heavy ion) or photon. In the case of a neutron as a projectile, the energy range starts just above the resonance region and extends up to a few hundreds of MeV for heavy ion induced reactions [20]. The code accounts for significant nuclear reaction mechanisms, such as direct, PC, and CN reactions. The statistical Hauser Feshbach formalism describes the CN decay with cascade and width fluctuations and the PC emission described by the classical exciton model [39]. EMPIRE-3.2 makes use of several codes, written by different authors, which were converted into subroutines and adapted for the present use. In most cases, the modifications concerned the input/output interface and never affected the physical model contained in the original source.

3.1.3 Talys-1.95(G) Code

The TALYS-1.95(G) code represents an enhanced iteration within the TALYS-1.95 code family [29]. It incorporates supplementary subprograms sourced from the ALICE and ALICE/ASH codes, specifically designed to handle pre-equilibrium emissions. Developed in the FORTRAN computer language, it stands as the final version for which strict adherence to the process of pre-equilibrium reaction. The TALYS-1.95(G) code is employed for the analysis and prediction of nuclear reactions involving neutrons, photons, protons, deuterons, tritons, ^{3}He-particles, and α-particles in the energy range of 1 keV to 200 MeV. It is applicable to target nuclides with a mass of 12 and heavier. The code incorporates optical, direct, CN (Compound Nucleus), PC (Pre-equilibrium) emission, and fission models. Equilibrium particle emission is described using the Hauser–Feshbach formalism [39]. TALYS-1.95 serves two primary purposes: first, as a tool in nuclear physics for analysing nuclear reaction experiments, facilitating the comparison between experimental and theoretical results to gain insights into fundamental particle-nuclei interactions [29]. Second, as a nuclear data tool, TALYS-1.95 can generate nuclear data for all open reaction channels within user-defined energy and angle ranges.

3.2. Formulations

3.2.1. Weiss Kopf-Ewing Formulation

At low incident energies the compound nucleus states are excited individually and each produces a resonance in the cross section that may be described by the Breit-Winger theory. As the incident energy increases compound nucleus states of higher energy are excited and these are closer to gather and of increasing width. Eventually they over lap and it is no longer possible to identify the individual Weiss Kopf-Ewing theory of compound nucleus reactions precedes the Hauser-Feshbach theory. These fluctuating features vanish in the energy average of the cross-section since these amplitudes are complex functions with random modulus and phase. The energy average of the cross-sections shows weak energy dependence and it is predictable by the theory [44].

To do this a reaction that proceeds from the initial channel α through the compound nucleus to the final channel β. Neglecting for the time being the formation of compound nucleus in different angular momentum J, the independence of formation and decay of the CN then gives for the cross-section [26, 51].

$$\sigma_{\alpha\beta} \approx \sigma_{CN}(\alpha)\frac{\Gamma_\beta}{\Gamma} \qquad (3.2)$$

Where $\sigma_{CN}(\alpha)$ is the cross-section for formation of the CN and, Γ_β and Γ are, the energy average width for the decay of the CN in channel β and the energy averaged total width respectively. From reciprocity theorem we can have that relates the cross section $\sigma_{\alpha\beta}$ to the cross section $\sigma_{\beta\alpha}$

$$g_\alpha k_\alpha^2 \sigma_{\alpha\beta} = g_\beta k_\beta^2 \sigma_{\beta\alpha} \qquad (3.3)$$

Where $g_\alpha = 2i_\alpha + 1$ and $g_\beta = 2i_\beta + 1$ are the statistical weights of the initial and final channels, i_α and i_β are the spin of the projectile and the ejectile, and k_α and k_β are their wave numbers. This gives,

$$g_\alpha k_\alpha^2 \sigma_{CN}(\alpha)\,\Gamma_\alpha = g_\beta k_\beta^2 \sigma_{CN}(\beta)\Gamma_\beta \qquad (3.4)$$

Or equivalently $$\frac{\Gamma_\alpha}{g_\alpha k_\alpha^2 \sigma_{CN}(\alpha)} = \frac{\Gamma_\beta}{g_\beta k_\beta^2 \sigma_{CN}(\beta)} \qquad (3.5)$$

Since the channels α and β are chosen arbitrarily, this relation holds for all possible channels so

$$\Gamma_\alpha \propto g_\alpha k_\alpha^2 \sigma_{CN}(\alpha) \qquad (3.6)$$

Since the total width is obtained by summing the Γ_α of overall open channels

$$\Gamma = \sum_\alpha \Gamma_\alpha \qquad (3.7)$$

The cross-section (3.3) becomes

$$\sigma_{\alpha\beta} = \sigma_{CN}(\alpha)\frac{g_\beta k_\beta^2 \sigma_{CN}(\beta)}{\sum_\alpha g_\alpha k_\alpha^2 \sigma_{CN}(\alpha)} \qquad (3.8)$$

Ejectiles with energy in the range ε_β to $\varepsilon_\beta + d\varepsilon_\beta$leave residual nucleus with energies in the range U_β to $U_\beta + dU_\beta$, where

$$U_\beta = E_{CN} - B_\beta - \varepsilon_\beta \qquad (3.9)$$

E_{CN} and B_β are respectively the CN energy and the binding of the ejectile in the CN. Introducing the density of levels of the residual nucleus $\omega(U_\beta)$ Eq (3.9) becomes

$$\sigma_{\alpha\beta} d\varepsilon_\beta = \sigma_{CN}(\alpha)\frac{g_\beta k_\beta^2 \sigma_{CN}(\beta)\omega(u)du_\beta}{\sum_\alpha \int_0^{E_\alpha^{max}} g_\alpha k_\alpha^2 \sigma_{CN}(\alpha)\omega(u_\alpha)du_\alpha} \qquad (3.10)$$

Or, since,$k^2 = 2m\varepsilon$

$$\sigma_{\alpha\beta} d\varepsilon_\beta = \sigma_{CN}(\alpha)\frac{(2i_\beta+1)u_\beta \varepsilon_\beta \sigma_{CN}(\beta)\omega(u_\beta)du_\beta}{\sum_\alpha \int_0^{E_\alpha^{max}} (2i_\alpha+1)u_\alpha \varepsilon_\alpha \sigma_{CN}(\alpha)\omega(u_\alpha)du_\alpha} \qquad (3.11)$$

Where u_α is the reduced mass of the ejectile α, this is the Weiss Kopf-Ewing formula for the angle integrated cross-sections. The corresponding general expression for the particle emission width is,

$$\Gamma_\beta = \frac{1}{\rho_{CN}(E_{CN})} \cdot \frac{(2i_\beta+1)u_{\beta_\beta}}{\pi^2 \hbar^2}\omega_\beta(\beta)\omega(u_\beta)d\varepsilon_\beta \qquad (3.12)$$

COMPLET code used the above equations in the predictions of reaction cross-sections following the formation of compound nucleus at some excitation energy and with some cross-section. The Weiss-Kopf calculation is then used with a 1-MeV grid size to perform the evaporation of a neutron, proton, alpha and deuteron storing the residual nucleus population into the appropriate bin. The control then moves over to the A-1 bin following neutrons emission, from the compound nucleus. This bin can also be resulted with the emission of proton, deuteron, and alpha particle. The residual nuclei obtained from the emission of aforesaid particles are stored in the respective bins. The code uses the number of millibarn in the highest energy bin A-1 and redistributes that cross-section in the same manner.

After this the control comes down to the next residual excitation bin and the process continues up to the moment all the cross-section redistributed and summed it in the appropriate bins of the residual nuclides. This logic is repeated going across the A as far as requested by an input parameter. After this the control comes down in Z to the nucleus A-1, Z-1 and repeats the process till all calculations is not completed for each input parameter [51].

3.2.2. Hauser-Feshbach Formulation

The Weiss Kopf- theory depends only on the nuclear level density and on the compounds nucleus formation cross-section which may be easily obtained from global optical model potentials. It is thus simple to use, but it has the disadvantage that it does not give the angular distribution of the emitted particles. This is provided by the Hauser-Feshbach theory. The Hauser-Feshbach theory gives the cross-sections that pass through a large number of CN states. The Bohr independence hypothesis can be used, together with some other simplified assumptions, to obtain an expressions for the total cross-section of a compound nucleus reaction.[44].

This theory takes into account the formation of the compound nucleus in states of different J and parity. Let us consider the case of a reaction leading from the initial channel α to final channel β. Since J and parity are good quantum numbers, the cross section is a sum of terms each corresponding to a given by [26, 52].

$$\sigma_{\alpha\beta} = \sum_{J,\pi} \sigma_{\alpha\beta}^{J\pi} \tag{3.13}$$

Averaging over the energy one further assumes the Bohr independent hypothesis holds for each $\sigma_{\alpha\beta}^{J\pi}$ thus,

$$\sigma_{\alpha\beta}^{J\pi} = \sigma_{CN}^{J\pi}(\alpha)\frac{\Gamma_{\beta}^{J\pi}}{\Gamma^{J\pi}} \tag{3.14}$$

Repeating the procedure used to obtain the Weiss Kopf-Ewing expression gives

$$\Gamma_{\beta}^{J\pi} \propto g_{\alpha}^{2}\sigma_{CN}^{J\pi}(\alpha) \tag{3.15}$$

Where now $g_\alpha = (2i_\alpha + 1)\,(2I_\alpha + 1)$ and i_α and I_α are, respectively, the projectile and target spin in channel α. If the process of pre-equilibrium emission is not taken in to consideration, the compound nucleus formation cross section (σ_{CN})

$$\sigma_{CN} = \sum_{J,\pi} \sigma_{CN}^{J\pi} \tag{3.16}$$

And the corresponding optical model reaction cross-section

$$\sigma_R = \frac{\pi}{k^2}\sum_{\ell}(2\ell+1)\,T_{\ell} \quad (3.17)$$

Considering J independent transmission coefficients $T_{\ell} = 1 - |\bar{S_{\ell}}|^2$ the reaction cross section may also be written as,

$$\sigma_R = \frac{\pi}{k^2}\sum_{\ell=0}^{\infty}\sum_{s=|I-1|}^{I+1}\sum_{J=|\ell-s|_{min}}^{\ell+1}\frac{(2J+1)T_{\ell}}{(2i+1)(2I+1)} \quad (3.18)$$

Where s, is the channel spin $s = I + i$

By rearranging the summation over different indexes, one gets;

$$\sigma_{CN} \approx \sigma_R = \frac{\pi}{k^2}\sum_J\frac{(2J+1)T_{\ell}}{(2i+1)(2I+1)}\sum_{s=|I-i|_{min}}^{I+i}\sum_{\ell=|J-s|_{min}}^{J+s}T_{\ell} \quad (3.19)$$

By comparing, Eq. (3.17) and Eq. (3.19) one can gets,

$$\frac{\Gamma_{\alpha}^{J\pi}}{\Gamma^{J\pi}} = \frac{\Gamma_{\alpha}{}^{J\pi}}{\sum_{\alpha}\Gamma_{\alpha}^{J\pi}} = \frac{\sum_{s,\ell}T_{\ell}(\alpha)}{\sum_{\alpha}\sum_{s,\ell}T_{\ell}(\alpha)} \quad (3.20)$$

Now the cross-sections in Eq. (3.14) for transition from the initial channel α to the final channel β may be written as,

$$\sigma_{\alpha\beta} = \frac{\pi}{k^2}\sum_J\frac{(2J+1)}{(2i_{\alpha}+1)(2I_{\alpha}+1)}\frac{\sum_{s,\ell}T_{\ell}(\alpha)\sum_{s',\ell'}T_{\ell'}(\beta)}{\sum_{\alpha}\sum_{s,\ell}T_{\ell}(\alpha)} \quad (3.21)$$

This is the Hauser-Feshback formula in its simplest form for the energy-average angle integrated cross-section of statistical reactions (reaction cross-section leading to a single final state).

If one interested on the cross section for populating all the available final states cross ponding to a given particles with energy between ε_{β} and$\varepsilon_{\beta} + d\varepsilon_{\beta}$, and a residual nucleus with energy between U_{β} and U_{β} +dU_{β}, where $U_{\beta} = E_{CN} - B_{\beta} - \varepsilon_{\beta}$. Assuming the spin dependent level density of residual nucleus with energy U_{β} and spin I_{β} may be factorized into the product of an energy dependent and a spin de-pendent term.

$$\omega_{\beta}(U_{\beta}, I_{\beta}) = \omega_{\beta}(U_{\beta})F(I_{\beta}) \quad (3.22)$$

And using

$$F(I) = (2I+1)\exp\left(-\frac{I(I+1)}{2\sigma^2}\right) \quad (3.23)$$

$\omega_\beta(U_\beta)$ Refers to level density, therefore theEq (3.21) becomes

$$\sigma_{\alpha\beta} = \frac{\pi}{k^2}\sum_J \frac{(2J+1)}{(2i_\alpha+1)(2I_\alpha+1)} \times$$

$$\frac{\sum_{s,\ell} T_\ell(\alpha) \sum_{s,'\ell'} T_{l'}(\beta) \sum_{I,\beta} \rho_\beta(U_\alpha)(2I_\beta+1)\exp(-\frac{I_\beta(I_\beta+1)}{2\sigma_\beta^2})}{\sum_\beta \int_0^{E^{\max\beta}} \sum_{s,\ell} T_\ell(\beta) \sum_{I\beta} \rho_\beta(U_\beta)(2I_\beta+1)\exp(-\frac{I_\beta(I_\beta+1)}{2\sigma_\beta^2}) du_\beta} \qquad (3.24)$$

This expression of the width for decay of CN, in state of energy E and spin J.

3.3. Person's Correlation Coefficient

Pearson's correlation coefficient R, measures the relationship's strength (direction and magnitude) between the theoretical predictions and experimental measurements of production cross sections [53, 54]. The Pearson's correlation coefficient R, is given by

$$R=\frac{\sum_{i=1}^{N}(X_{T_i}-<X_T>)(X_{E_i}-<X_E>)}{(N-1)(S_{XT})(S_{XE})} \qquad (3.25)$$

Where;

$$< X_T >= \frac{1}{N}\sum_i^N (X_{T_i}) \qquad (3.26)$$

$$S_{XT} = \sqrt{\frac{1}{N-1}\sum_{i=1}^{N}(X_{T_i}-< X_T >)} \qquad (3.27)$$

$$< X_E >= \frac{1}{N}\sum_{i=1}^N (X_{E_i}) \qquad (3.28)$$

$$S_{XE} = \sqrt{\frac{1}{N-1}\sum_{i=1}^{N}(X_{E_i}-< X_E >)} \qquad (3.29)$$

Where R is correlation coefficient and unit less, $\langle X_T \rangle$ and $\langle X_E \rangle$ are the mean theoretical and experimental reaction cross-sections respectively, X_{T_i} and X_{E_i} are the theoretical and experimental total cross-sections of ith value respectively. N is the number of the theoretical and experimental data, S_{XT} and S_{XE} are the standard deviation of the theoretical and experimental total cross-sections respectively [55]. In general, R returns a unit less value between −1 and 1. A value of +1 indicates a strong and positive relationship, −1 indicates a strong and negative relationship, and 0 indicates no relationship. If $0 \leq R \leq 0.3$, the correlation is weak and positive, $0.3 \leq R \leq 0.7$ describes moderate correlation and $0.7 \leq R \leq 1$, the correlation is strong.

Chapter Four

Result and Discussions

In this work, we studied the production cross-sections of medically important ^{88}Y, ^{89}Zr, ^{90}Y, and ^{99}Mo radionuclides produced in the interactions of α-projectile with ^{89}Y and ^{96}Zr -target at ≈10-60 MeV of α-energy. Theoretical predictions of cross-sections were carried out using the reaction model codes COMPLETE, TALYS-1.95(G), and EMPIRE 3.2. These codes were selected because they have been very successful and widely used for predicting production cross-sections and reaction data evaluation work [4, 39, 40].

A comparison of theoretically predicted production cross-sections was made with the experimentally measured cross-section data available in the EXFORE database [21, 56, 57, 58, 62]. To strengthen analysis of the present work, Pearson's correlation relations were used to provide quantitative associative strength between the theoretical predictions and experimental measurements of the production cross-sections. Table 1-3 displays the calculated Pearson's correlation coefficients for presently studied medically used radionuclides.

i) Analysis using COMPLETE code

COMPLETE code is an advanced version of the ALICE code family with new physics finding, correction, and capabilities and has been used for the prediction of production cross-sections, especially for the production of medical radionuclides [4, 50, 64, 65]. In this code, the level density parameter a, which predominantly affects the equilibrium state components of a cross-section, is calculated from the expression a = A/K MeV, where A is the nucleon number of a compound system, and K is an adjustable constant, which may be varied to match the experimental data [30]. For representative ^{89}Y (α, x) ^{88}Y reaction, the values of K (K = 8, 10, and 12) were varied to fit the experimental data. As can be seen from Figure 4.1(a) up to 34.48MeV, the region where the maximum cross-section is attained, picks an area of the cross-sections with a value of K=10, in general, reproduced satisfactorily experimentally measured cross-section values. Another sensitive input parameter, initial exciton number, n_o, which represents the initial configuration of particles and holes, was also varied n_o (n_o = 4, 5, and 6) to fit the measured cross section. It may be seen from figure 4.1(b) for the same ^{89}Y (α, x) ^{88}Y reaction the initial exciton number n_o = 4 better reproduced the measured data up to the pick point.

Furthermore, the mean free path multiplier (MFM), another sensitive input parameter in the COMPLETE code, is also varied MFM = (1, 2, and 2.5) to fit the experimentally measured cross-section data for the same reaction channel ^{89}Y (α, x) ^{88}Y. As can be seen from Figure 4.1(c), up to the pick region, a value of MFPM=1 satisfactorily reproduced the experimentally measured cross-section values.

For the remaining medical radionuclides produced in the interaction of α-projectile with ^{89}Y, and ^{96}Zr-target, a combination of parameter values K=12, n_o=4, and MFPM=1 were used in COMPLETE code predictions.

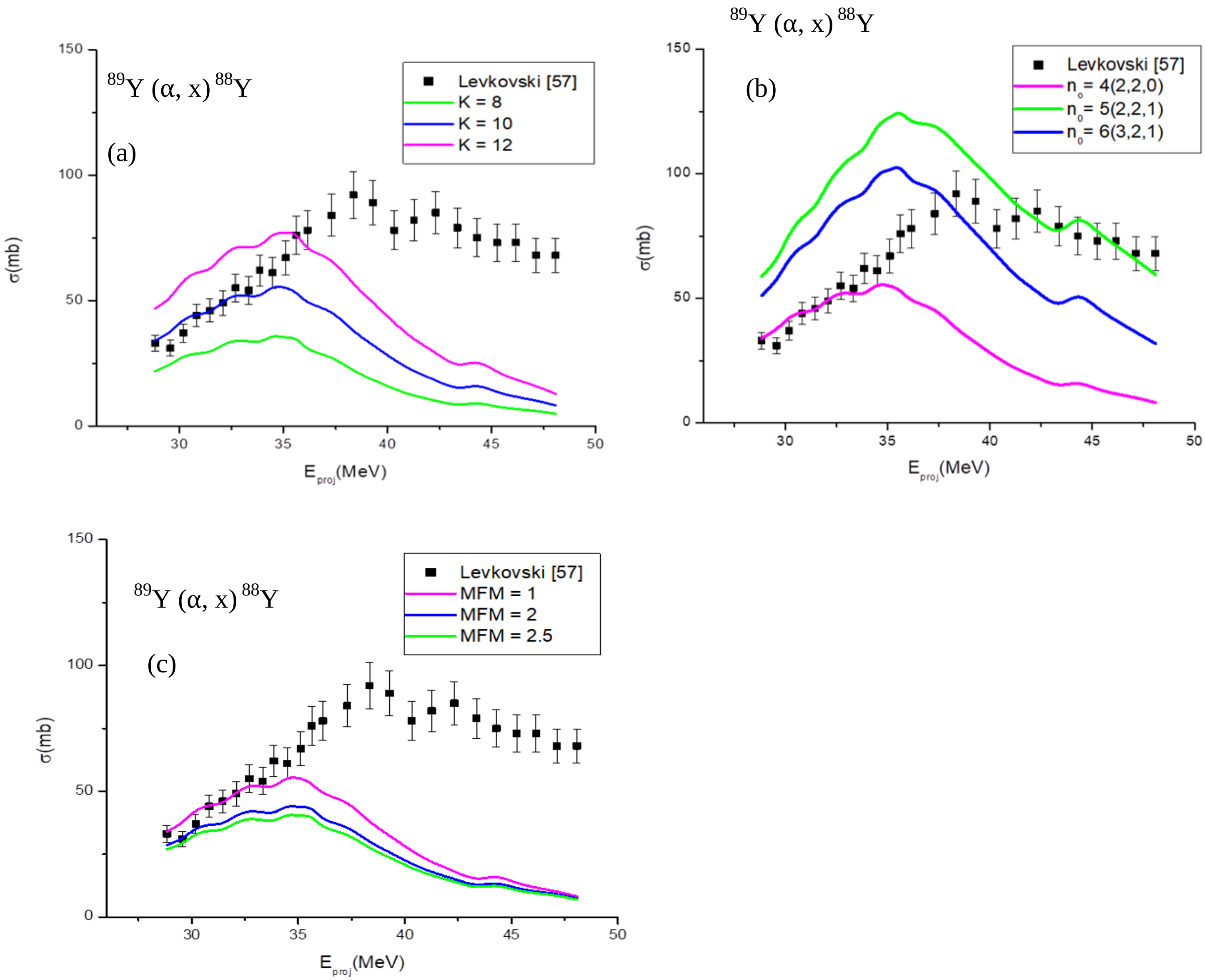

Figure 4.1 experimentally measured and theoretically predicted excitation function of ^{88}Y radionuclides.

ii) Analysis with TALYS-1.95(G) and EPIRE-3.2 codes

The advanced versions of the TALYS-1.95(G) and EMPIRE 3.2 codes use different level density models to predict production cross-sections. In the present production cross-section predictions, we used the Enhanced Generalized Superfluid Model in the EMPIRE 3.2 code and the Exciton model with optical model transition rates in the TALYS-1.95(G) code. These models from the respective reaction codes were selected because they have successfully predicted production cross-sections [20].

4.1. Production of Medically important Radionuclides

4.1.1. ^{88}Y Radionuclide

Medically important ^{88}Y produced via (α, x) channel in the interaction of α-projectile with ^{89}Y-target is a radioactive isotope with a relatively long half-life of approximately 106.6 days, undergoing primarily β^+-decay. In this process, a proton in the nucleus transforms into a neutron, emitting a positron and a neutrino. This decay characteristic makes it valuable for medical applications, particularly in positron emission tomography (PET) scans, which can be used to detect and provide detailed images of metabolic processes within the body [59].

Figure.4.2 displayed the measured cross section along with theoretical predictions for ^{88}Y radionuclide produced via (α, x) channel in the interaction of α-projectile with ^{89}Y. As can be seen in Figure.4.2, the predicted cross-section values using TALYS-1.95(G) are in good agreement with the measured values of Levkovski [57]. On the other hand except in 28.84-34.48MeV the predictions of both COMPLETE and EMPIRE-3.2 codes underestimate the measurement of Levkovski [57]. Further, it may be observed from figure 4.2 that, the theoretical predictions underestimate the measurements of Singh et al. [56]. The maximum production cross-section value for ^{88}Y radionuclide produced via (α, x) channel obtained using TALYS-1.95(G) code is about ≈ 86.7 mb at ≈ 39 MeV.

It may further be observed from Table 1 Pearson's correlation coefficient values confirmed a strong positive correlation between theoretically predicted production cross-sections and experimentally measured value of Singh et al., [56]. However, except for the prediction of TALYS-1.95(G) the Pearson’s correlation coefficient values of COMPLETE and EMPIRE-3.2 confirmed negative correlation with experimental value of Levkovski [57].

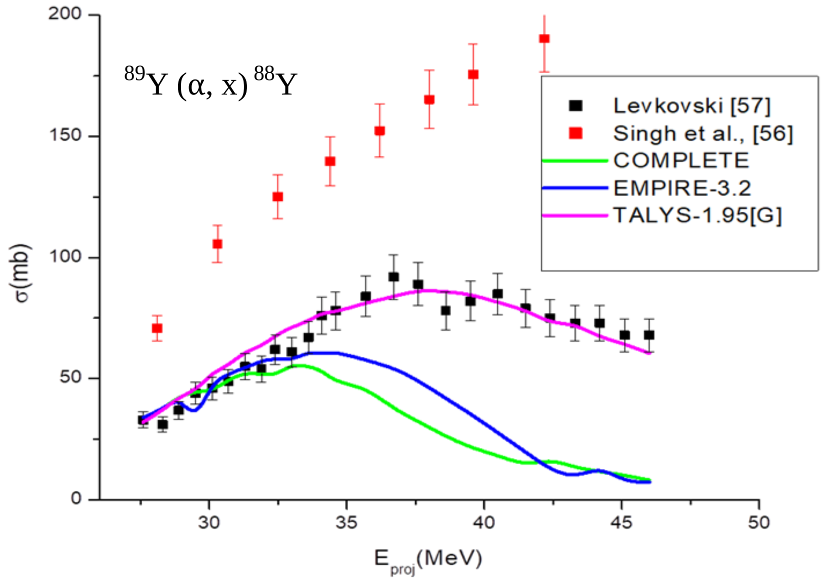

Figure 4.2 experimentally measured and theoretically predicted excitation function of ^{88}Y radionuclides.

4.1.2. ^{99}Mo Radionuclide

The ^{99}Mo radionuclide that can be produced significantly in the interaction of α-projectile with ^{96}Zr is a crucial radionuclide widely used in the field of nuclear medicine due to its decay properties and significant medical applications. It has a relatively short half-life of about 66 hours and decays via β^- emission to ^{99m}Tc, a metastable nuclear isomer. The decay process involves the emission of β particles and γ rays, transforming into ^{99m}Tc, which is the most utilized radiotracer in diagnostic imaging. ^{99m}Tc emits gamma rays suitable for detection by medical imaging equipment, enabling it to highlight bodily structures and functions in scans such as SPECT (Single Photon Emission Computed Tomography). This makes ^{99}Mo indispensable for creating ^{99m}Tc generators, which are used in hospitals worldwide to diagnose a variety of conditions, including heart disease, cancer, and bone disorders [61].

Figure 4.3 displayed the experimentally measured production cross sections and the theoretical predictions for ^{99}Mo radionuclide produced via (α, n) channel. It may be seen from this figure that the COMPLETE code predicted cross-section values are in good agreement with the experimentally measured values of Chowdhury et al. [58]. However, except at the initial two energy points the predicted cross section value by using TALYS-1.95(G) code underestimate the measurements of chowdhury et al., [58].

It may be further observed from Figure 4.3, above ≈ 24.8MeV energy points, the predictions of COMPLETE and EMPIRE 3.2 codes showed discrepancies with the measured values of Chowdhury et al., [58] although the shapes of the excitation functions showed similar trend. Furthermore, it may be observed from Figure 4.3 that, except at the initial two energy points, the theoretical predictions underestimates the measurements of Puppilo et al. [21].

The production cross sections for medically important ^{99}Mo radionuclide obtained using the COMPLETE code have a peak value of about ≈ 135mb at ≈ 14 MeV. It may further be observed from table 2 Pearson's correlation coefficient values confirmed moderate and strong positive correlation between the experimentally measured and theoretically predicted production cross-sections.

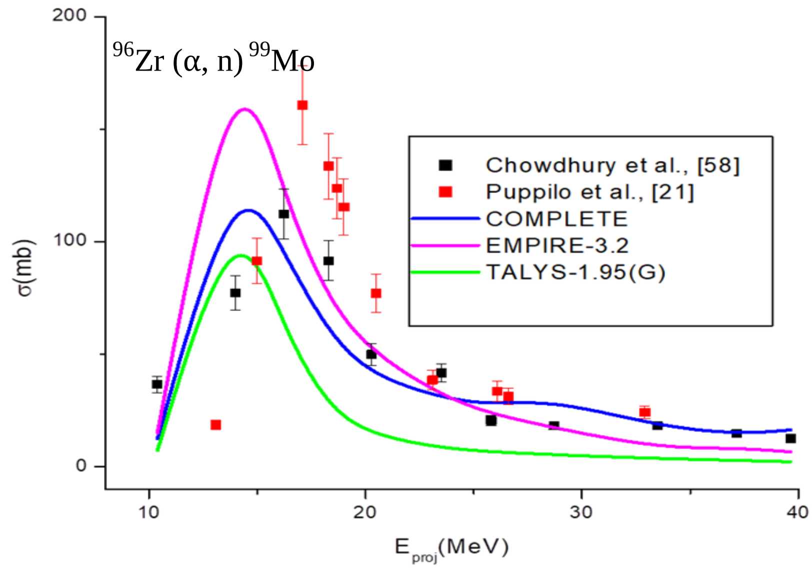

Figure 4.3 experimentally measured and theoretically predicted excitation function of ^{99}Mo radionuclides.

4.1.3. ^{89}Zr Radionuclide

^{89}Zr is gaining significant attention in the field of nuclear medicine due to its favorable physical and chemical properties, particularly for applications in immuno-PET, a technique that combines the sensitivity of PET imaging with the specificity of monoclonal antibodies targeting cancer cells. Its half-life of 78.4 hours is optimally suited for studies of slower biological processes, such as the accumulation and retention of labeled antibodies in tumors, which typically take several days to peak, aligning well with the pharmacokinetics of most antibodies used in oncology. The β^+decay of ^{89}Zr emit positrons, which annihilate with electrons to produce gamma rays detectable by PET scanners.

This feature allows for high-resolution, three-dimensional imaging of tumors and metastases in the body, providing vital information on tumor size, location, and activity. The extended half-life of ^{89}Zr not only facilitates prolonged imaging periods but also enables transportation to sites without local radiopharmaceutical production facilities, thus broadening its accessibility and use in clinical trials and routine diagnostics [63].

The measured production cross-sections, along with the theoretical predictions for ^{89}Zr radionuclide produced via $^{89}Y(\alpha, x)^{89}Zr$ reaction, are shown in Figure 4.4. It may be observed from this figure that the predicted cross-section values using COMPLETE and TALYS-1.95(G) code are in good agreement with the measured values of Shahid et al. [62]. However, except at ≈ 35 MeV, the predictions of EMPIRE3.2 code overestimate the measured values of Shahid et al., [62] although the shapes of the two excitation functions showed similar trends. Further, it may be observed from Figure 4.4 that the theoretically predicted cross-section values, in general, overestimate the measurements of Levkovski [57], although the shapes of the excitation functions showed a similar trend. It is worth mentioning that COMPLETE and TALYS-1.95(G) codes better predicted the measurements of Levkovski [57] than the EMPIRE3.2 code.

The production cross sections for medically important ^{89}Zr radionuclide obtained using the TALYS-1.95(G) code has a peak value of about ≈ 139 mb at ≈ 44.91 MeV. As shown in table 1 and 3 Pearson's correlation coefficient values confirmed a strong positive correlation between the experimentally measured and theoretically predicted production cross-sections.

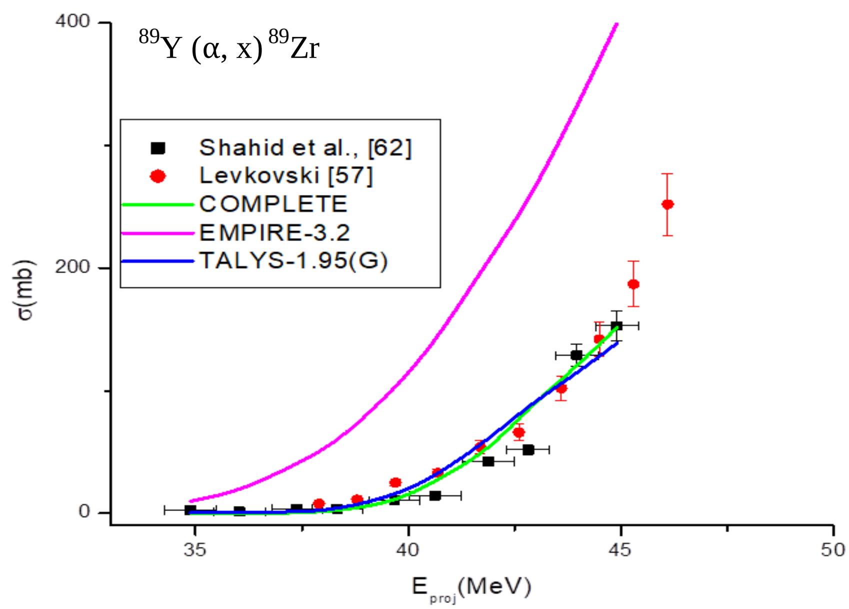

Figure 4.4 experimentally measured and theoretically predicted excitation function of ^{89}Zr radionuclides.

4.1.4. ^{90}Y Radionuclide.

Theoretically predicted and experimentally measured excitation functions for ^{90}Y radionuclide produced in the interaction of α -projectile with ^{89}Y target via the (α, x) channel are shown in Figure 4.5. ^{90}Y is highly valued in the medical field due to its potent therapeutic properties, particularly in the areas of cancer treatment and management of certain rheumatologic conditions. The radionuclide's relatively short half-life of 64 hours is optimal for therapeutic applications where a rapid but intense radiation dose is required. The β^- decay of ^{90}Y produces high-energy electrons that have a maximum energy of 2.28 MeV, providing a deep penetration of about 2.5 to 11 mm in tissue, which is ideal for targeting and destroying cancer cells while minimizing exposure to surrounding healthy tissues. ^{90}Y primary application is in radio embolization, often used for the treatment of unrespectable liver tumors [60].

As can be seen from Figure 4.5 the predicted cross-section values using TALYS-1.95(G) code are in good agreement with the measured values of Shahid et al., [62]. It may be observed from figure 4.5 that except at the last energy points, the predicted cross section obtained from using COMPLETE is satisfactorily in good agreement with experimental measured values of Shahid et al., [62]. Further, it may be observed from Figure 4.5 that the prediction of EMPIRE 3.2 code overestimates the measurements of Shahid et al., [62] although the shapes of the two excitation functions showed a similar trend in the entire energy range. The maximum production cross-section value for ^{90}Y radionuclide produced via (α, x) channel obtained using TALYS-1.95(G) code is about ≈ 5.2mb at ≈44.9MeV. As shown in Table 3, the Pearson's coefficient confirmed a strong positive correlation between the theoretical predictions and the measurements of Shahid et al. [62].

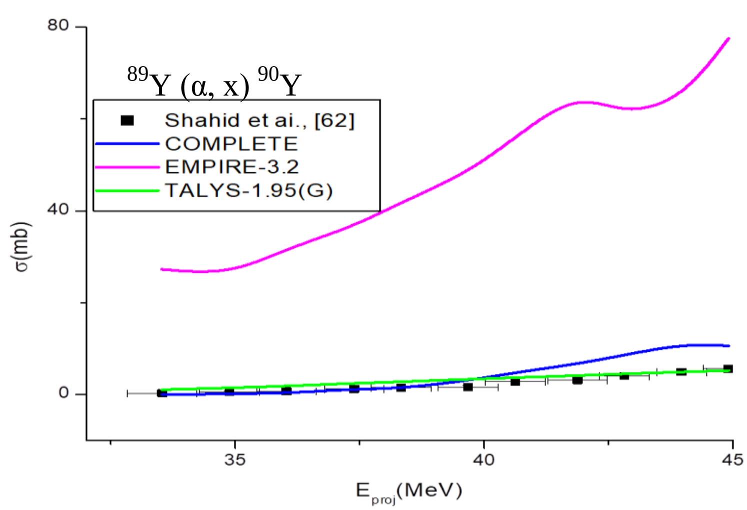

Figure 4.5 experimentally measured and theoretically predicted excitation function of ^{90}Y radionuclides.

Table 1-3 lists Pearson's correlation values between different experimental measurements by different groups and present theoretical predictions. R values without and within brackets, square brackets represent the correlation between COMPLETE and experimental, EMPIRE-3.2 and experimental, and TALYS-1.95(G) and experimental, respectively.

Table1. Pearson's correlation coefficient values between theoretical predictions and experimental measurements of ^{88}Y, ^{89}Zr radionuclides

Radionuclides	Levkovski [57]	Singh et al., [56]
^{88}Y	-0.3446, (-0.06), [0.9565]	0.9872, (0.8987), [0.9876]
^{89}Zr	0.9917, (0.9923), [0.9906]	- - -

Table2. Pearson's correlation coefficient values between the theoretical predictions and experimental measurements ^{99}Mo radionuclide.

Radionuclide	Chowdhury et al., [58]	Puppilo et al., [21]
^{99}Mo	0.7942, (0.7886), [0.6864]	0.6123, (0.5928), [0.4425]

Table3. Pearson's correlation coefficient values between the theoretical prediction and experimental measurements ^{89}Zr, ^{90}Y radionuclides.

Radionuclides	Shahid et al., [62]
^{89}Zr	0.976, (0.948), [0.9613]
^{90}Y	0.987, (0.951), [0.9651]

Chapter Five

Conclusion

Theoretical predictions were made using COMPLETE, EMPIRE-3.2 and TALYS-1.95(G) reaction model codes for the production of medically important ^{88}Y, ^{89}Zr, ^{90}Y and ^{99}Mo radionuclides produced in the interaction of α-projectile with ^{89}Y and ^{96}Zr-targets at ≈10-60 MeV. The predicted results were compared and discussed with the experimental data available in the EXFORE database. The TALYS-1.95(G) code predicted and measured cross sections for the productions of medically important ^{88}Y, ^{90}Y, and ^{89}Zr radionuclide, in general, are found to be in good agreement over the entire energy range except for ^{99}Mo radionuclide. Pearson's statistical coefficients confirmed a strong positive correlation between TALYS-1.95(G) codes predicted and experimentally measured cross section except for ^{99}Mo. On the other hand, Pearson's correlation coefficient values between COMPLETE and EMPIRE-3.2 predicted and experimentally measured production cross-sections confirmed weak to strong correlations. Furthermore, it was found that the TALYS-1.95(G) predicted and experimentally measured production cross-sections in general attained maximum values below ≈45MeV α-energy for medically important ^{88}Y, ^{90}Y, and ^{89}Zr radionuclides produced via complex (α,x) channel. Thus the obtained result can be used as reference cross-section data for optimized production of medically important ^{88}Y, ^{90}Y, ^{89}Zr and ^{99}Mo radionuclides using single α + ^{89}Y, ^{96}Zr system.

References

[1]. Arnould, M., & Goriely, S. (2020). Astronuclear Physics: A tale of the atomic nuclei in the skies. *Progress in Particle and Nuclear Physics*, *112*, 103766.

[2]. Qaim, S. M., Spahn, I., Scholten, B., & Neumaier, B. (2016). Uses of alpha particles, especially in nuclear reaction studies and medical radionuclide production. *Radiochimica acta*, *104*(9), 601-624.

[3]. Taddesse, A. (2007). *The Study Of α-Particle Induced Reaction on Gallium Isotopes* (Doctoral dissertation, Addis Ababa University).

[4]. Yigit, M., 2020. Study on (n, p) reactions of 58, 60, 61, 62,64Ni using new developed empirical formulas. Nuclear Engineering and Technology 52, 791–796.

[5]. Qaim, S.M., 2011. Development of novel positron emitters for medical applications. Nuclear and radiochemical aspects. Radiochim. Acta 99, 611.

[6]. Qaim, S.M.; Capote, R.; Tarkanyi, F. (2011). *Nuclear Data for the Production of Therapeutic Radionuclides*; Trs 473; International Atomic Energy Agency: Vienna, Austria, Volume 395.

[7]. Nayak, D., & Lahiri, S. (1999). Application of radioisotopes in the field of nuclear medicine: I. Lanthanide series elements. *Journal of radio analytical and nuclear chemistry*, 242(2), 423-432

[8]. Alsharef, S. H. O. M. O. K. H., Alanazi, M. A. S. H. A. E. L., Alharthi, F. A. T. I. M. A. H., Qandil, D. A. N. A., & Qushawy, M. O. N. A. (2020). Review about radiopharmaceuticals: preparation, radioactivity, and applications. *Int J App Pharm*, 12(3), 8-15

[9]. Takács, S., Aikawa, M., Haba, H., Komori, Y., Ditrói, F., Szűcs, Z. & Ukon, N. (2020). Cross sections of alpha-particle induced reactions on natNi: production of 67Cu. *Nuclear Instruments and Methods in Physics Research Section B: Beam Interactions with Materials and Atoms*, 479, 125- 136

[10]. Mushtaq, A., & Qaim, S. M. (1990). Excitation functions of α-and 3He-particle induced nuclear reactions on natural germanium: evaluation of production routes for 73Se. *Radiochemical Acta*, 50(1-2), 27-32

[11]. Aslam, M.N., Qaim, S.M., 2014b. Nuclear model analysis of excitation functions of p, d and α-particle induced reactions on (64) Zn and (3) He - and α - particle induced reactions on (59) Co leading to formation of copper-61: comparison of major production routes. Appl. Radiat. Isot. 94, 131–140.

[12]. Aytekin, H., Baldik, R., 2013. Pre-equilibrium cross section calculations in alpha induced reactions on 32S, 64Zn, 67Zn, 89Y, 90Zr and 153Eu targets used for production of 32P, 64Cu, 67Cu, 89Sr, 90Y and 153Sm therapeutic radionuclides. Ann. Nucl. Energy 53, 439–446.

[13]. Hoefnage, Cornelis A., 1998. Radionuclide cancer therapy. Ann. Nucl. Med. 12, 61–70

[14]. Karamyan, S.A., et al., 1992. Activation of Aluminum Foils by He-4 Ions at 25-45. Int. Conf.Nucl.Spectroscopy Nucl.Struct.,Alma-Ata, p.291

[15]. Ismail, M., 1993. Measurement of excitation functions and mean projected recoil ranges of nuclei in alpha- induced reactions on F,Al,V,Co and Re nuclei. Pramana 40, 227

[16]. Murata, T., Aikawa, M., Saito, M., Haba, H., Komori, Y., Ukon, N & Ditrói, F. (2019). Excitation function measurement for zirconium-89 and niobium-90 production using alphainduced reactions on yttrium-89. *Nuclear Instruments and Methods in Physics Research Section B: Beam Interactions with Materials and Atoms*, 458, 21-27

[17]. Aikawa, M., Saito, M., Ukon, N., Komori, Y., & Haba, H. (2018). Activation cross sections of alpha-induced reactions on natIn for 117mSn production. *Nuclear Instruments and Methods in Physics Research Section B: Beam Interactions with Materials and Atoms*, 426, 18-21

[18]. Tárkányi, F. T., Ignatyuk, A. V., Hermanne, A., Capote, R., Carlson, B. V., Engle, J. W., ... & Verpelli, M. (2019). Recommended nuclear data for medical radioisotope production: diagnostic positron emitters. *Journal of Radio analytical and Nuclear Chemistry*, 319(2), 533-666

[19]. Aslam, M. T., Ali, W., & Hussain, M. (2021). Nuclear model analysis of the 65Cu (α, n) 68Ga reaction for the production of 68Ga up to 40 MeV. Applied Radiation and Isotopes, 170, 109590

[20]. Amanuel, F. K. (2021). Nuclear model prediction for production of medical ^{22}Na, ^{51}Cr, ^{60}Co, ^{61}Cu, ^{64}Cu, ^{65}Zn, ^{67}, ^{68}Ga, ^{88}Y and ^{99}Mo radionuclides: Comparison of experimental and theoretical data. *Applied Radiation and Isotopes*, 172, 109674

[21]. Pupillo, G., Esposito, J., Gambaccini, M., Haddad, F., & Michel, N. (2014). Experimental cross section evaluation for innovative 99Mo production via the (α, n) reaction on 96 Zr target. *Journal of Radioanalytical and Nuclear Chemistry, 302*, 911-917

[22]. Aslam, M.N., Qaim, S.M., 2014a. Nuclear model analysis of excitation functions of p, d and α- particle induced reactions on nickel isotopes for production of the medically interesting copper-61. Appl. Radiat. Isot. 89, 63–73.

[23]. Zaneb, E., Hussain, M., Amjad, N., Qaim, S.M., 2016. Evaluation of nuclear reaction cross section data for the production of 87Y and 88Y via p, d and α - particle induced transmutations. Appl. Radiat. Isot. 112, 69–79. https://doi.org/10.1016/j. apradiso.2016.03.016.

[24]. L'Annunziata, M. F. (2020). The atomic nucleus, nuclear radiation, and the interaction of radiation with matter. In *Handbook of Radioactivity Analysis* (pp. 1-243). Academic Press

[25]. Alemu, m. (2020). *Study of proton induced reaction on rhodium isotope at various projectile energy* Doctoral dissertations, Mekdes Alemu

[26]. Aubrecht, G. (2003). A teacher's guide to the nuclear science wall chart. *Contemporary Physics Education Project*

[27]. Shehata, M. M. M. (2011). *Radiochemical Studies Relevant to Cyclotron Production of the Radionuclides* 71, 72As, 76, 77, 80mBr (Doctoral dissertation, Universität zu Köln

[28]. Nigussie, B. (2012). *Complete and incomplete fusion studies in some* 14N+ 59Co *systems* (Doctoral dissertation, Addis Ababa University).

[29]. Choudhary, M., Sharma, A., Gandhi, A., Singh, N., & Kumar, A. (2020), et al., Study of pre-equilibrium contributions in proton spectra of 59Co (n, x p) reaction using TALYS-1.9.

[30]. Schunck, N., & Regnier, D. (2022). Theory of nuclear fission. *Progress in Particle and Nuclear Physics, 125*, 103963.

[31]. Asres, Y. H., Mathuthu, M., & Ferede, Y. A. (2019). Investigation of nuclear reaction mechanisms of Nickel isotopes at various energies induced by alpha particles. *Journal of Physics Communications*, *3*(11), 115018.

[32]. Scheid, W. (2009). Nuclear Reactions. *FUNDAMENTALS OF PHYSICS-Volume III*, 166

[33]. Satchler, G. R., & Satchler, G. R. (1990). *Introduction to nuclear reactions* (pp. 21-88). Palgrave Macmillan UK

[34]. HEAVY-ION, C. P. I. R. (2012). Karl-Heinz Kampert. *Nuclear Matter and Heavy Ion Collisions*, *205*, 287

[35]. Erhardt, P. (2009). Drug discovery. In *Pharmacology* (pp. 475-560). Academic Press

[36]. Kamal, A. (2014). Nuclear Reactions. In *Nuclear Physics* (pp. 425-502). Berlin, Heidelberg: Springer Berlin Heidelberg

[37]. Hedlund, A. (2011). *Incorporating nuclear reactions into SEU prediction* (Master's thesis).

[38]. Rowe, D. J., & Wood, J. L. (2010). *Fundamentals of nuclear models: foundational models*. World Scientific Publishing Company.

[39]. Herman, M., Capote, R., Sin, M., Trkov, A., Carlson, B. V., Oblozinsky, P. ... & Zerkin, V. (2013). *EMPIRE-3.2 Malta modular system for nuclear reaction calculations and nuclear data evaluation User's Manual* (No. BNL-101378-2013). Brookhaven National Lab. (BNL), Upton, NY (United States). National Nuclear Data Center (NNDC).

[40]. Capote, R., Herman, M., Obložinský, P., Young, P. G., Goriely, S., Belgya, T., ... & Talou, P. (2009). RIPL–reference input parameter library for calculation of nuclear reactions and nuclear data evaluations. *Nuclear Data Sheets*, *110*(12), 3107-3214.

[41]. Yiğit, M., & Kara, A. (2017). Model-based predictions for nuclear excitation functions of neutron-induced reactions on 64, 66− 68Zn targets. *Nuclear Engineering and Technology*, *49*(5), 996-1005.

[42]. Konobeyev, A. Y., Fischer, U., Koning, A. J., Pereslavtsev, P. E., & Blann, M. (2011). Implementation of the geometry dependent hybrid model in TALYS. J. *Korean Phys*. Soc, 59, 9

[43]. Issa, S. A. A. M. (2009). Cross Section for Residual Nuclide Production by Proton–Induced Reaction with Heavy Target Elements at Medium Energies. PhD thesis

[44] Hodgson, P. E. (1987). Compound nucleus reactions. *Reports on Progress in Physics*, *50*(9), 1171.

[45]. Hilaire, S. (2004). Energy dependence of the level density parameter. *Physics Letters B*, *583*(3-4), 264-268.

[46]. Olorunsola, A. B., Bamikole, J. A., Bello, A. A., & Ige, O. O. (2023). Theoretical prediction of neutron-induced radiative capture cross section on some isotopes of minor actinides from 10 keV-10 MeV. Journal of Nuclear and Radiation Sciences, 1, 1-11.

[47]. Mengoni, A., & Nakajima, Y. (1994). Fermi-gas model parametrization of nuclear level density. *Journal of Nuclear Science and Technology*, *31*(2), 151-162.

[48]. Baur, G., Bertulani, C. A., & Rebel, H. (1986). Coulomb dissociation as a source of information on radiative capture processes of astrophysical interest. *Nuclear Physics A*, *458*(1), 188-204

[49]. Younes, Walid; Loveland, Walter (2021). *An Introduction to Nuclear Fission*. Springer. pp. 10, 25–26, 56–58

[50]. Kara, A., et al., 2015. Modeling study on production cross sections of 11In radioisotoes used in nuclear medicine. Kerntechnik 80 (3), 270–274.

[51]. Hodgson, P. E., Gadioli, E., & Erba, E. G. (1997). Introductory Nuclear Physics, Clarendon

[52]. Girma, A. and G. Fessahatsion, Investigating entrance channel influences in the fusion of some heavy–ion systems. J Appl Biotechnol Bioeng, 2019. 6(5): p. 247-252.

[53]. Schober, P., Boer, C., & Schwarte, L. A. (2018). Correlation coefficients: appropriate use and interpretation. Anesthesia & analgesia, 126(5), 1763-1768.

[54]. Wang, J. (2012). On the relationship between Pearson correlation coefficient and Kendall's tau under bivariate homogeneous shock model. International Scholarly Research Notices, 2012.

[55]. Sedgwick, P. (2012). Pearson's correlation coefficient. BMJ 345 (jul04 1): 4483.

[56]. Singh, N. L., Gadkari, M. S., & Chintalapudi, S. N. (2000). Measurement and analysis of alpha particle induced reactions on yttrium. *Physica Scripta*, *61*(5), 550.

[57]. Levkovskij, V. N. (1991). Activation cross section nuclides of average masses (A= 40–100) by protons and alpha-particles with average energies (E= 10–50 MeV). *Moscow, Russia*.

[58]. Chowdhury, D. P., Pal, S., Saha, S. K., & Gangadharan, S. (1995). Determination of cross section of α-induced nuclear reaction on natural Cr and Zr by stacked foil activation for thin layer activation analysis. *Nuclear Instruments and Methods in Physics Research Section B: Beam Interactions with Materials and Atoms*, *103*(3), 261-266.

[59]. Christian, P. E., & Waterstram-Rich, K. M. (2013). *Nuclear Medicine and PET/CT-E-Book: Nuclear Medicine and PET/CT-E-Book*. Elsevier Health Sciences

[60]. O'Malley, J. P., & Ziessman, H. A. (2020). *Nuclear Medicine and Molecular Imaging: The Requisites E-Book: Nuclear Medicine and Molecular Imaging: The Requisites E-Book*. Elsevier Health Sciences

[61]. Schöder, H., Erdi, Y. E., Larson, S. M., & Yeung, H. W. (2003). PET/CT: a new imaging technology in nuclear medicine. *European journal of nuclear medicine and molecular imaging*, *30*, 1419-1437

[62]. Shahid, M., Kim, K., Naik, H., Zaman, M., Kim, G., Yang, S. C., & Song, T. Y. (2015). Measurement of excitation functions in alpha-induced reactions on yttrium. *Nuclear Instruments and Methods in Physics Research Section B: Beam Interactions with Materials and Atoms*, *342*, 158-165.

[63]. Deri, M. A., Zeglis, B. M., Francesconi, L. C., & Lewis, J. S. (2013). PET imaging with 89Zr: from radiochemistry to the clinic. *Nuclear medicine and biology*, *40*(1), 3-14.

[64]. Yigit, M., Tel, E., 2014. Nuclear model calculation for production of 18F, 22Na, 44,46Sc, 54Mn, 64Cu, 68Ga, 76Br and 90Y radioniclides used in medical applications. Ann. Nucl. Energy 69, 44–50.

[65]. Tel, E., Yigit, M., Tanir, G., 2012. Study on (n,t) reactions on Zr, Nb and Ta nuclei. J. Fusion Energy 31, 184–190.

Appendix

Table4. Experimentally and theoretical predicted cross section data of medically important ^{88}Y radionuclide.

A(X1)	B(Y1)	C(Y eror)	D(X2)	E(X eror)	F(Y2)	G(Y eror)	complete	empire	talys
27.6	33	3.3	28.1	0.5	70.8	5.1	33.97	33.9764	32.0533
28.3	31	3.1	30.3	0.5	105.6	7.6	37.26	37.484	36.937
28.9	37	3.7	32.5	0.5	125.1	9	42.74	42.5052	42.3612
29.5	44	4.4	34.4	0.4	139.8	10	44.6	32.7678	45.1948
30.1	46	4.6	36.2	0.4	152.4	10.9	44.91	48.3658	52.3351
30.7	49	4.9	38	0.4	165.3	11.9	49.62	52.0039	55.5056
31.3	55	5.5	39.6	0.4	175.6	12.6	52.45	54.4958	61.1964
31.9	54	5.4	42.2	0.4	190.4	13.7	51.84	57.3592	63.3639
32.4	62	6.2	44.5	0.4	202.3	14.5	51.41	58.339	67.8196
33	61	6.1	46.8	0.4	211.8	15.2	55.97	57.6112	71.3267
33.6	67	6.7	--	--	--	--	55.16	61.1328	73.6884
34.1	76	7.6	--	--	--	--	53.35	60.4365	77.2727
34.6	78	7.8	--	--	--	--	48.54	61.1199	77.5338
35.7	84	8.4	--	--	--	--	46.35	57.6667	81.3774
36.7	92	9.2	--	--	--	--	37.54	54.4867	83.8598
37.6	89	8.9	--	--	--	--	32.31	49.221	86.6703
38.6	78	7.8	--	--	--	--	26.16	41.8555	85.9143
39.5	82	8.2	--	--	--	--	21.64	35.4876	84.8767
40.5	85	8.5	--	--	--	--	18.22	27.6379	81.4785
41.5	79	7.9	--	--	--	--	14.19	19.7285	78.3497
42.4	75	7.5	--	--	--	--	16.83	12.4475	72.9026
43.3	73	7.3	--	--	--	--	13.31	8.9417	72.6316
44.2	73	7.3	--	--	--	--	11.63	13.8439	67.0301
45.1	68	6.8	--	--	--	--	10.17	7.38257	64.4057
46	68	6.8	--	--	--	--	8.156	7.19244	60.4563

Table5. Experimentally and theoretical predicted cross section data of medically important ^{99}Mo radionuclide.

A(X1)	B(Y1)	C(Y1 eror)	D(X2)	E(X2 eror)	F(Y2)	G(Y2 eror)	complete	empire	talys
10	36.6	3.6	13.1	1.5	18.7	2.1	12.49	15.1864	7.32498
13.5	77.3	7.7	15	1.4	91.6	10	135.4	195.963	120.73
15.6	112.3	11.1	17.1	1.3	160.8	17.6	95.21	119.725	60.5512
17.6	91.6	8.8	18.3	1.2	133.7	14.6	58.77	73.146	25.7118
19.5	50	4.8	18.7	1.2	123.8	13.5	40.57	50.7883	14.1311
22.6	41.7	3.9	19	1.1	115.5	12.6	30.57	31.5864	8.34402
24.8	20.6	2.1	20.5	1.1	77.1	8.4	27.58	23.533	6.72881
27.6	18.3	1.7	23.1	1	36.8	4.3	29.79	17.3401	5.34346
32.2	18.4	1.8	26.1	0.9	33.6	4.4	18.14	8.25985	3.71908
35.7	14.8	1.5	26.6	0.9	31.3	3.7	14.43	8.47853	2.85014
38.1	12.6	1.5	32.9	0.8	24.2	2.9	16.44	6.69434	2.45333

Table6. Experimentally and theoretical predicted cross section data of medically important ^{89}Zr radionuclide

A(X1)	B(X1 eror)	C(Y1)	D(Y1 eror)	E(X2)	F(Y2)	G(Y2 eror)	complete	empire	talys
33.53	0.6	2.6	0.5	37.9	7.9	0.79	0	9.97285	0.3593
34.88	0.6	1.5	0.2	38.8	11.3	1.13	0	17.8899	0.63638
36.03	0.6	3.7	0.7	39.7	25	2.5	0.2004	40.5924	1.1495
37.39	0.6	3.8	0.3	40.7	33	3.3	2.052	57.7572	3.06924
38.33	0.6	10.4	1	41.7	54	5.4	9.041	101.527	14.347
39.68	0.6	14.5	1.1	42.6	66	6.6	26.09	139.302	30.0466
40.63	0.6	42.4	3.2	43.6	102	10.2	50.76	206.7	60.0864
41.88	0.5	51.9	4	44.5	142	14.2	85.79	253.497	87.7462
43.97	0.5	129	9	45.3	187	18.7	120.2	331.878	114.4335
44.2	0.5	153	12	46.1	252	25.2	151.7	400.252	139.033

Table7. Experimentally and theoretical predicted cross section data of medically important ^{90}Y radionuclide

A(X1)	B(X1 eror)	C(Y1)	D(Y1 eror)	complete	empire	talys
33.53	0.7	0.3	0.1	0.00422	27.2569	1.05688
34.88	0.6	0.6	0.2	0.116	26.0553	1.41714
36.03	0.6	0.7	0.1	0.3261	31.7448	1.83413
37.39	0.6	1.2	0.3	1.161	36.6325	2.43082
38.33	0.6	1.5	0.2	1.323	41.8131	2.76707
39.68	0.6	1.6	0.4	3.051	48.3088	3.32288
40.63	0.6	2.8	0.3	4.781	56.0532	3.69315
41.88	0.6	3.1	0.4	6.649	65.8975	4.13617
42.82	0.5	4	0.3	8.602	60.8061	4.52435
43.97	0.5	4.9	0.5	10.98	64.1544	4.92628
44.91	0.5	5.6	0.5	10.61	77.4783	4.65456